Bulletin of the Seismological Society of America, Vol. 106, No. 1, pp. –, February 2016, doi: 10.1785/0120140244

Long-Period Ground-Motion Prediction Equations for Moment Magnitude Estimation of Large Earthquakes in Japan

by Rami Ibrahim, Hongjun Si, Kazuki Koketsu, and Hiroe Miyake

Abstract We developed long-period (5–30 s) ground-motion prediction equations (GMPEs) for peak ground velocities (PGVs) and peak ground displacements (PGDs) for crustal, interplate, and intraplate earthquakes. We used strong-motion data from KiK-net downhole stations located in layers with shear-wave velocities equal to or greater than 2000 m/s. The data set consisted of 20 earthquakes of $6 \leq M_w \leq 9.1$ that occurred in and around Japan, including the 2011 Tohoku earthquake. Two-stage regression analyses were performed to derive the long-period GMPEs. We fitted the data with bilinear regression lines bending at M_w 7.5, although additional factors such as focal depth and earthquake type were found to enhance the fitting with the observed data. The developed equations indicated that long-period PGVs and PGDs are larger for crustal earthquakes than for interplate and intraplate earthquakes. The attenuation coefficients indicated that long-period PGVs and PGDs increase with increasing depth. We estimated the moment magnitude by fitting the observed PGVs and PGDs in the 5–30 s period range with the long-period GMPEs. We obtained estimates of the magnitudes of 23 earthquakes recorded by KiK-net downhole accelerometers, and the results were consistent with the moment magnitudes obtained from the Global Centroid Moment Tensor project. The described method was proven useful for estimating the moment magnitude of great earthquakes, offering the potential for rapid estimation of moment magnitude if information from the source area is available.

Introduction

Rapid estimation of the moment magnitude (M_w) of great earthquakes (e.g., the 2004 Sumatra, Indonesia, 2010 Maule, Chile, and 2011 Tohoku, Japan, earthquakes) is an important issue in seismology, earthquake engineering, and natural-hazard assessment. Traditional magnitude scales such as the surface-wave magnitude M_s and the Japan Meteorological Agency (JMA) magnitude M_{JMA} suffer from saturation for large earthquakes (Heaton *et al.*, 1986), which makes scaling for such earthquakes unstable. For instance, because of saturation, the scaling of M_s (developed according to surface waves of 20 ± 2 s periods from shallow-focus earthquakes within a distance of 15°–130°; Gutenberg, 1945) reaches a maximum value of about M_s 8.6 (Purcaru and Berckhemer, 1978). The M_{JMA} magnitude scaling uses a waveform filtered with a cutoff period at 5 s; therefore, any phase with period ≤ 5 s may be used for the M_{JMA} calculation (Katsumata, 1996). M_{JMA} provides a reasonable indication of the sizes of earthquakes of $M_w < 8.0$ (Heaton *et al.*, 1986). This highlights the importance of using periods > 5 s for scaling earthquakes of $M_w > 8.0$. In contrast, M_w is stable for large earthquakes. M_w as proposed by Kanamori (1977) and Hanks and Kanamori (1979) is defined as

$$M_w = \frac{2}{3} \log M_0 - 10.7, \qquad (1)$$

in which M_0 is the seismic moment in dyn·cm and M_0 is calculated using methods such as centroid moment tensor (CMT) solutions (Dziewonski *et al.*, 1981) or *W* phase (Kanamori and Rivera, 2008). However, these methods are sophisticated, and M_w is usually determined from long-period teleseismic waveforms recorded by global broadband stations. A few hours are required for data acquisition and magnitude estimation before issuing a correct magnitude. In the context of rapidly evolving information from the global earthquake response community, which includes both internal and publicly distributed products, Hayes *et al.* (2011) have explained the 88 hr response timeline of the National Earthquake Information Center after the 2011 Tohoku earthquake. Following the 2011 Tohoku earthquake, attempts have been undertaken to shorten the time required to estimate M_w for large earth-

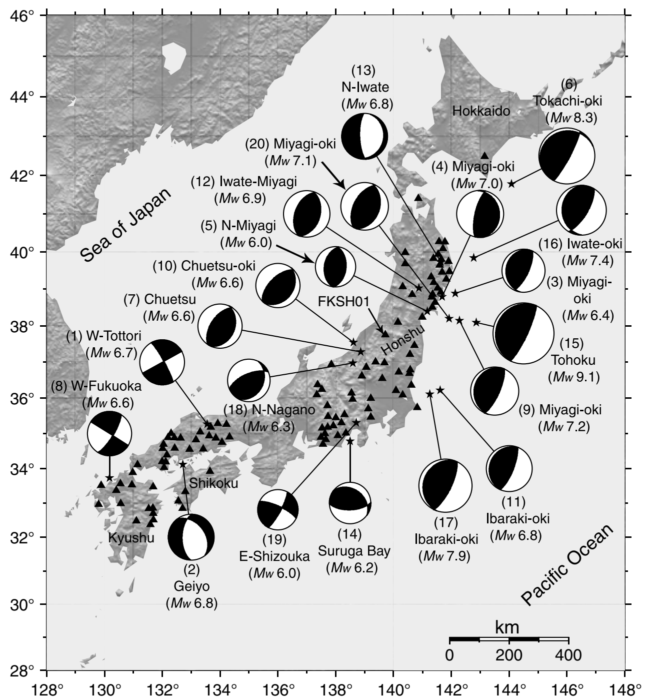

Figure 1. Epicenters (black stars) and focal mechanisms of the earthquakes used in this study. The focal mechanisms were obtained from the Global Centroid Moment Tensor (CMT) project. Black triangles indicate the KiK-net station sites.

quakes. For instance, Ohta *et al.* (2012) used Global Positioning System data to develop a displacement detection and estimation algorithm called Real-time Automatic detection method for Permanent Displacement (RAPiD). They determined that an estimated M_w of 8.7 for the 2011 Tohoku earthquake was released 4 min 35 s after the earthquake origin time. However, this value is still an underestimate of the final M_w of 9.1.

Considering the simple equations for the estimation of peak ground motion that are used for rapid determination of M_s or M_{JMA}, we develop here a simple equation to estimate M_w, based on peak ground motions of hard-rock sites, that compensates for the magnitude saturation experienced by the M_s and M_{JMA} scales. Japan has densely distributed strong-motion stations such as the K-NET and KiK-net networks, operated by the National Institute of Earth Science and Disaster Prevention (NIED; Kinoshita, 1998; Aoi *et al.*, 2004). These networks faithfully record the ground motion of large earthquakes and, therefore, develop a nonsaturated magnitude scaling. Moreover, the entire record from a near-field strong-motion network is obtained within a few minutes of the occurrence of an earthquake, which accelerates the magnitude estimation.

Large earthquakes usually generate longer-period ground motions than do smaller earthquakes. Many observational and theoretical studies have been conducted to improve under-

Table 1
Earthquake Data Used to Develop Long-Period Ground-Motion Prediction Equations and Reference Source Model Used to Estimate the Fault Distance (FD) and Equivalent Hypocentral Distance (EHD)

Number	Earthquake	Origin time (yyyy/mm/dd hh:mm)	Longitude (°)	Latitude (°)	Depth (km)	M_w	Earthquake Type	Reference Source Model
1	Western Tottori	2000/10/06 13:30	133.55 E	35.27 N	11	6.7	Crustal	Iwata and Sekiguchi (2002)
2	Geiyo	2001/03/24 15:58	132.71 E	34.12 N	51	6.8	Intraplate	Yagi and Kikuchi (2002)
3	Miyagi-Oki	2002/11/03 12:37	142.14 E	38.89 N	46	6.4	Interplate	EIC Seismological Note Number 128
4	Miyagi-Oki	2003/05/26 18:24	141.68 E	38.80 N	71	7.0	Intraplate	Aoi *et al.* (2003)
5	Northern Miyagi	2003/07/26 07:13	141.17 E	38.40 N	12	6.0	Crustal	Hikima and Koketsu (2004)
6	Tokachi-Oki	2003/09/26 04:50	144.08 E	41.78 N	42	8.3	Interplate	Koketsu *et al.* (2004)
7	Chuetsu	2004/10/23 17:56	138.87 E	37.29 N	13	6.6	Crustal	Horikawa (2005)
8	Western Fukuoka	2005/03/20 10:53	130.18 E	33.73 N	9	6.6	Crustal	Asano and Iwata (2006)
9	Miyagi-Oki	2005/08/16 11:46	142.28 E	38.15 N	42	7.2	Interplate	Wu *et al.* (2008, 2009)
10	Chuetsu-Oki	2007/07/16 10:13	138.61 E	37.55 N	17	6.6	Crustal	Irikura (2008)
11	Ibaraki-Oki	2008/05/08 01:45	141.61 E	36.22 N	51	6.8	Interplate	Nagoya University (2008)*
12	Iwate–Miyagi Nairiku	2008/06/14 08:43	140.88 E	39.03 N	8	6.9	Crustal	Suzuki *et al.* (2010)
13	Northern Iwate	2008/07/24 00:26	141.64 E	39.73 N	108	6.8	Intraplate	Suzuki *et al.* (2009)
14	Suruga Bay	2009/08/11 05:07	138.50 E	34.78 N	23	6.2	Intraplate	Suzuki and Aoi (2009)
15	Tohoku	2011/03/11 14:46	142.86 E	38.10 N	24	9.1	Interplate	Y. Yokota *et al.* (2011)
16	Iwate-Oki	2011/03/11 15:09	142.78 E	39.84 N	32	7.4	Interplate	JMA
17	Ibaraki-Oki	2011/03/11 15:15	141.26 E	36.11 N	43	7.9	Interplate	Satoh†
18	Northern Nagano	2011/03/12 03:59	138.60 E	36.98 N	8	6.3	Crustal	Takeda (2011)
19	Eastern Shizuoka	2011/03/15 22:31	138.71 E	35.31 N	14	6.0	Crustal	JMA
20	Miyagi-Oki	2011/04/07 23:32	141.92 E	38.20 N	66	7.1	Intraplate	JMA

JMA, Japan Meteorological Agency.
*Research Center for Seismology, Volcanology and Disaster Mitigation, Graduate School of Environmental Studies, Nagoya University (2008).
†Source model information obtained from T. Satoh (personal comm., 2012).

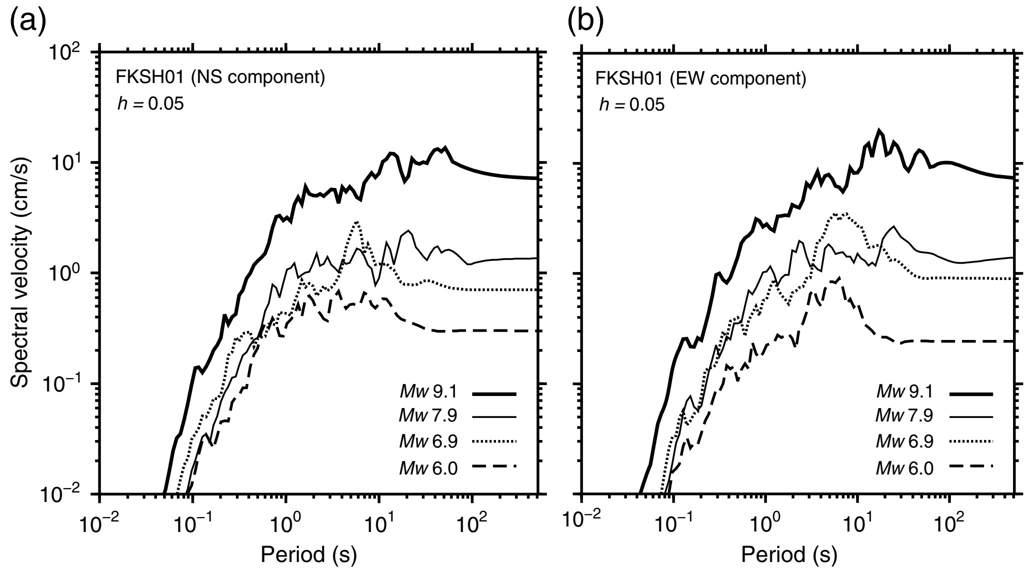

Figure 2. The 5% damped spectral velocity at FKSH01 borehole accelerometer station for (a) north–south and (b) east–west components. The ground-motion records of the 2003 northern Miyagi (M_w 6.0), 2008 Iwate–Miyagi Nairiku (M_w 6.9), 2011 Ibaraki-Oki (M_w 7.9), and 2011 Tohoku (M_w 9.1) earthquakes were used in this study.

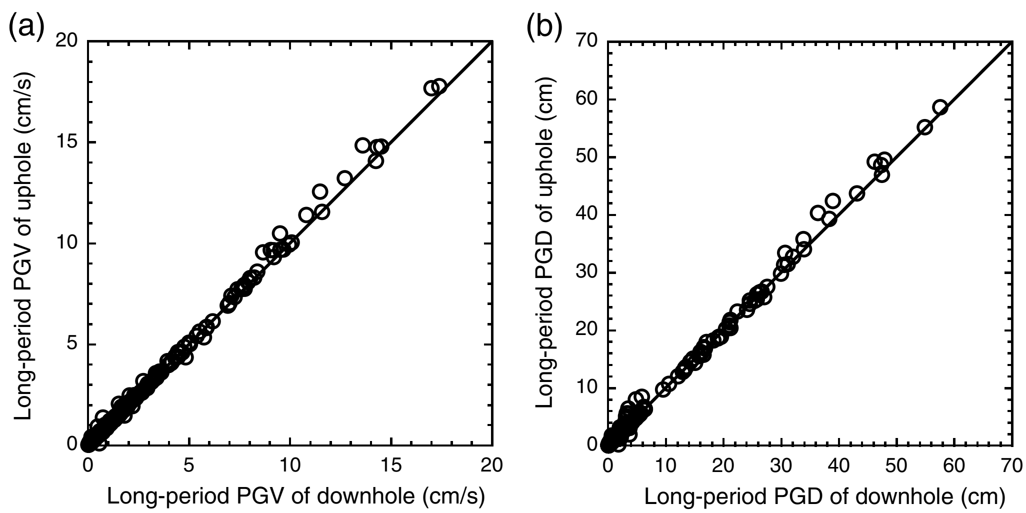

Figure 3. Comparison of long-period (a) peak ground velocities (PGVs) and (b) peak ground displacements (PGDs) recorded at the KiK-net downhole and uphole seismometers.

standing of the characteristics of long-period ground motions (e.g., Hanks, 1976; Kanamori, 1979; Somerville and Graves, 1993; Koketsu and Miyake, 2008); however, few studies have evaluated the long-period spectral characteristics of ground shaking based on actual data. Using a worldwide data set of crustal earthquakes, the Next Generation Attenuation project (NGA-West and NGA-West 2) of the Pacific Earthquake Engineering Research Center studied 5% damped spectral acceleration up to 10 s (e.g., Abrahamson and Silva, 2008; Boore and Atkinson, 2008; Campbell and Bozorgnia, 2008, 2014; Chiou and Youngs, 2008, 2014; Idriss, 2008, 2014; Abrahamson *et al.*, 2014; Boore *et al.*, 2014). However, data related to subduction earthquakes were not included in the development of either the NGA-West or the NGA-West 2 models. Kataoka *et al.* (2008), T. Yokota *et al.* (2011), and Yuzawa and Kudo (2011) proposed long-period ground-motion prediction equations (GMPEs) of 1% or 5% damped acceleration response spectra at periods between 1 or 2 and 15 or 20 s, using strong-motion records observed in Japan. Dhakal *et al.* (2013) used strong-motion data from K-NET and KiK-net to develop GMPEs of 5% damped absolute velocity response of 1–10 s for early warning of long-period

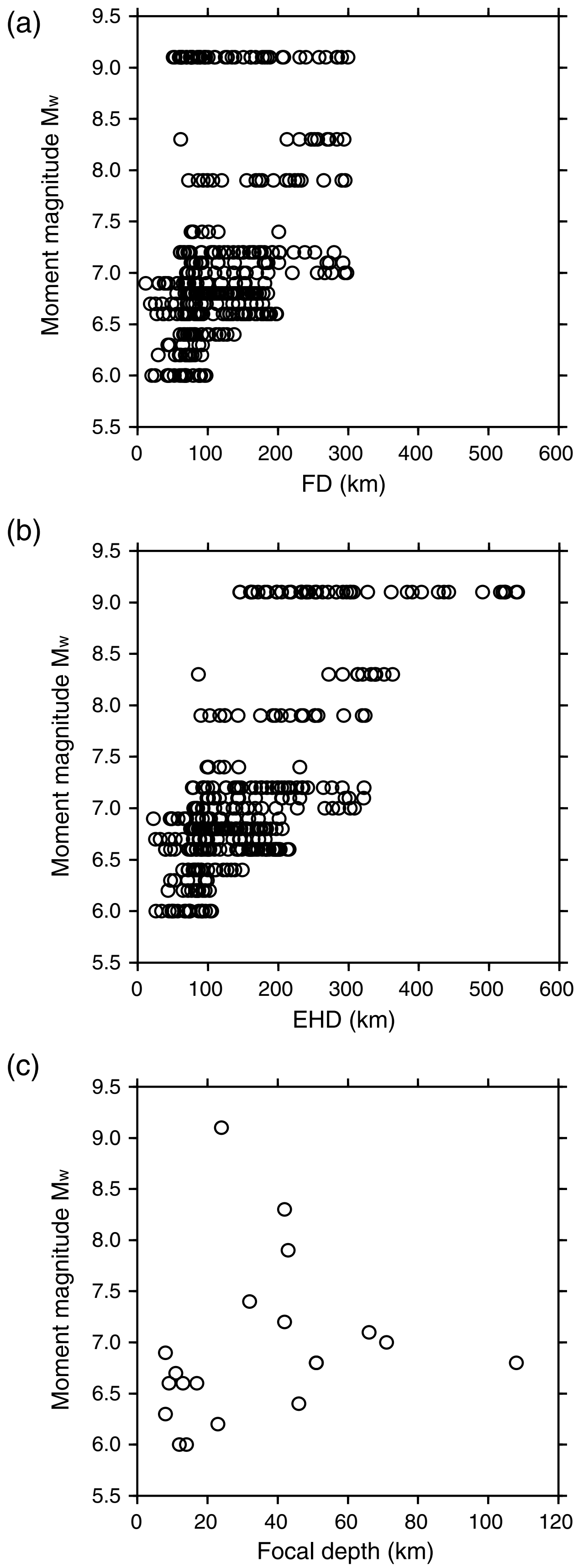

Figure 4. Distribution of magnitude with (a) fault distance (FD), (b) equivalent hypocentral distance (EHD), and (c) focal depth.

ground motions. Despite their importance for hazard assessment, GMPEs have not been developed for long-period peak ground motions such as the peak ground velocities (PGVs) or peak ground displacements (PGDs) in Japan.

Here we developed long-period GMPEs for PGVs and PGDs based on downhole KiK-net data in which the accelerometers are located on hard-rock layers with minimal influence of site effects. Our interest is in the 5–30 s period range, which is most appropriate for scaling both the moderate and large earthquakes of our data set. We considered the differences in magnitude scaling between moderate and large earthquakes, based on scaling of seismic source spectra, to overcome the saturation for large earthquakes. Then, we estimated M_w for large earthquakes by fitting the observed long-period PGVs and PGDs to the developed long-period GMPEs. We validated our method by comparing our M_w estimates with those of the Global CMT project solutions.

Strong-Motion Data Set

We collected data from 20 moderate and large earthquakes that occurred in and around Japan for which sufficient records and source information were available (Table 1 and Fig. 1). The values of M_w for these earthquakes ranged from 6.0 to 9.1, and the focal depths were 8–108 km. The earthquakes selected were of crustal, interplate, and intraplate types. Crustal earthquakes occur within the crust at focal depths ≤ 20 km, such as the 2004 Chuetsu (M_w 6.6) and 2008 Iwate–Miyagi Nairiku (M_w 6.9) earthquakes. Interplate earthquakes such as the 2011 Tohoku earthquake (M_w 9.1) occur at the interface between a subducting and an overriding plate. Intraplate earthquakes, for example, the 2003 Miyagi-Oki earthquake (M_w 7.0), occur within a subducting plate and have focal depths > 50 km, with the exception of the 2009 Suruga Bay earthquake (M_w 6.2), which had a focal depth of 23 km. Based on this classification, our data set consists of eight crustal, seven interplate, and five intraplate earthquakes (Table 1).

We used KiK-net strong-motion data from downhole instruments located on bedrock layers where the shear-wave velocity (V_S) was ≥2000 m/s and site effects are expected to be negligible. Accelerometers provide good estimates of ground motion at periods up to and exceeding 30 s (Boore, 2005; Wang *et al.*, 2007; Paolucci *et al.*, 2008). Prior to processing the data, we investigated the predominant long periods by performing velocity spectral analysis. Figure 2 shows an example of the 5% damped spectral velocity calculated using strong-motion data from the FKSH01 borehole seismometer. The seismometer at this site is located on hard rock, for which $V_S = 2600$ m/s. Figure 2 presents the spectral velocity of the records from the 2003 northern Miyagi (M_w 6.0), 2008 Iwate–Miyagi Nairiku (M_w 6.9), 2011 Ibaraki-Oki (M_w 7.9), and 2011 Tohoku (M_w 9.1) earthquakes. Periods of 1–50 s are mostly dominant in the spectral velocity, and periods tend to become longer as

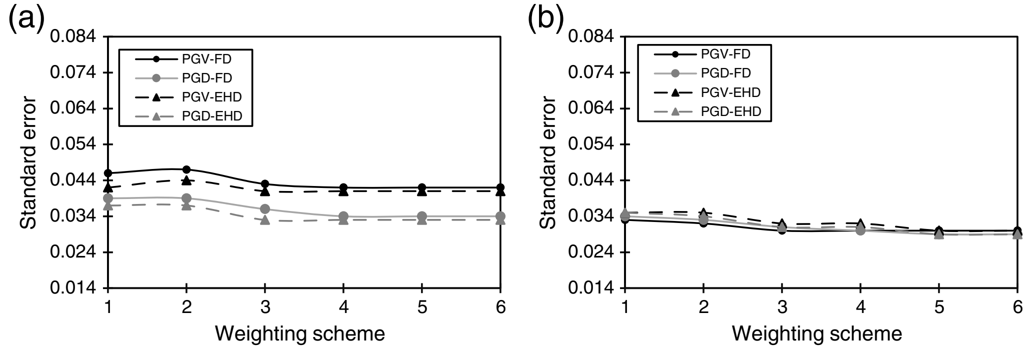

Figure 5. Standard error versus weighting scheme for the (a) 2000 western Tottori and (b) 2008 Iwate–Miyagi Nairiku earthquakes. Numbers on the abscissa refer to the weighting scheme used, as follows: (1) no weighting; (2) $[4(X \le 25),\ 2(25 < X \le 50),\ 1(50 < X \le 100),\ 1(X > 100)]$; (3) $[6(X \le 25),\ 3(25 < X \le 50),\ 2(50 < X \le 100),\ 1(X > 100)]$; (4) $[8(X \le 25),\ 4(25 < X \le 50),\ 2(50 < X \le 100),\ 1(X > 100)]$; (5) $[12(X \le 25),\ 4(25 < X \le 50),\ 2(50 < X \le 100),\ 1(X > 100)]$; and (6) $[16(X \le 25),\ 4(25 < X \le 50),\ 2(50 < X \le 100),\ 1(X > 100)]$, for the four cases PGVs versus FDs, PGDs versus FDs, PGVs versus EHDs, and PGDs versus EHDs.

the earthquake size increases. Because our primary aim was to estimate the magnitude of large earthquakes, it was necessary to filter the records with the correct period range to scale the waveforms without saturation. As mentioned previously, the JMA magnitude scale is calculated from waveforms with periods ≤ 5 s; herein, we chose periods ≥ 5 s. For

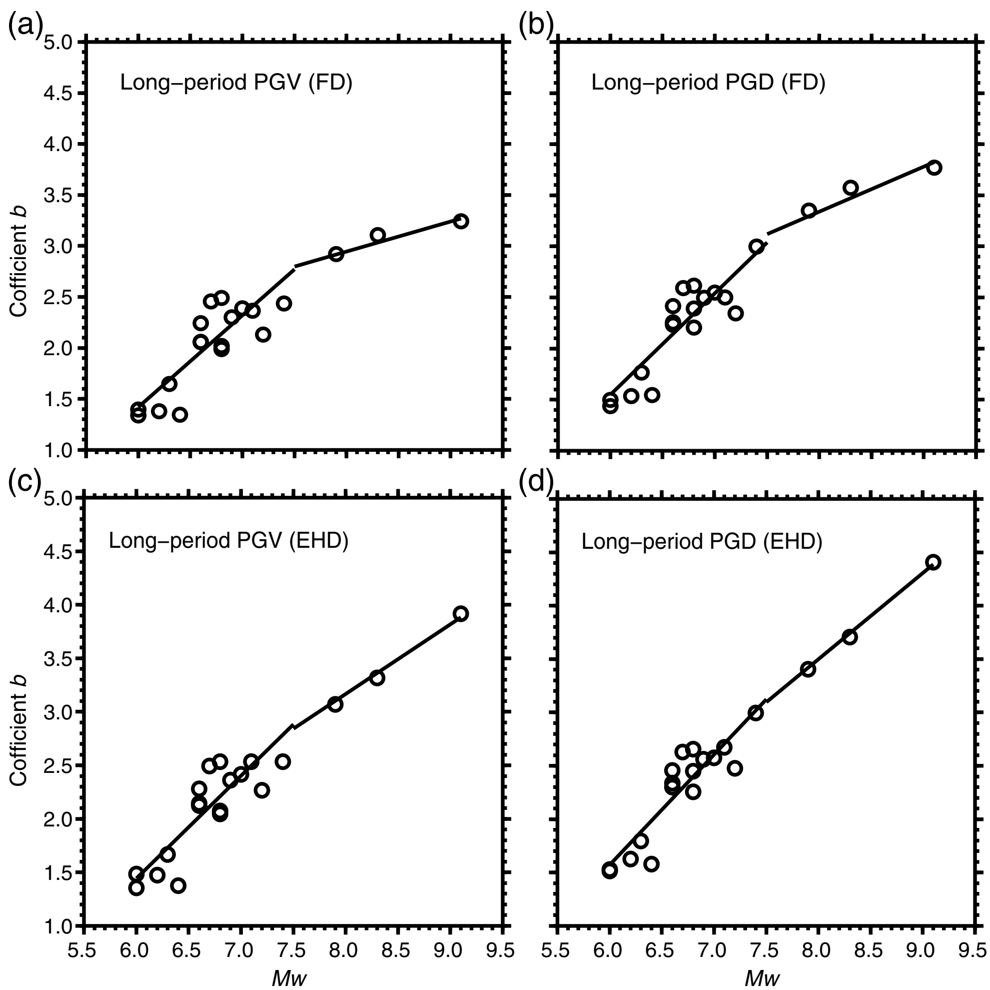

Figure 6. Scaling of coefficient b with respect to M_w using the results for long-period (a) PGVs versus FDs, (b) PGDs versus FDs, (c) PGVs versus EHDs, and (d) PGDs versus EHDs.

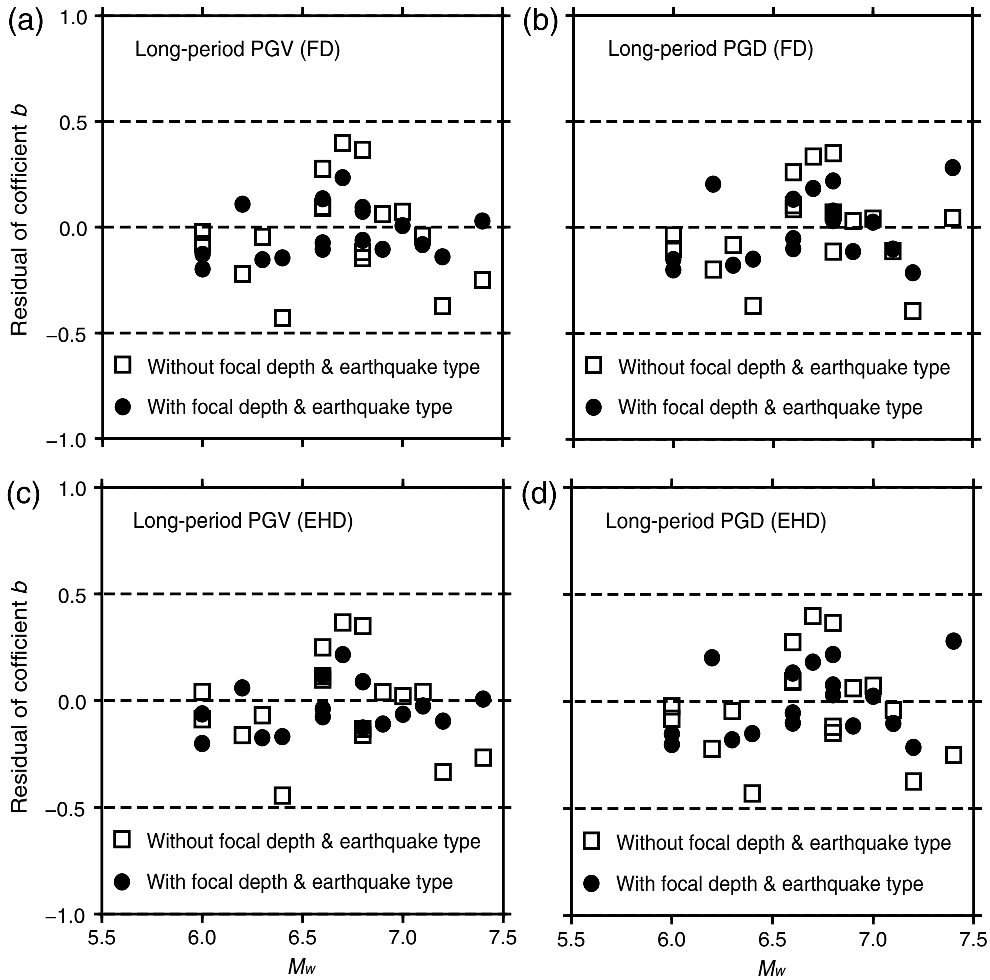

Figure 7. Comparison of residuals of coefficient b before (solid circles) and after (squares) consideration of focal depth and earthquake type for long-period (a) PGVs versus FDs, (b) PGDs versus FDs, (c) PGVs versus EHDs, and (d) PGDs versus EHDs.

the different periods tested, we found that periods up to 30 s better represented the ground motion for the largest-magnitude earthquakes in our data set. For periods > 30 s, background noise generated artifacts during the integration process of acceleration to the velocity and displacement records, particularly for moderate earthquakes. Thus, a Butterworth band-pass filter with cutoff periods of 5–30 s was applied to the entire data set. Subsequently, we obtained the long-period PGV and PGD values as the peak square root of the sum of squares of the two orthogonal horizontal components. Comparison between uphole and downhole records of long-period PGVs and PGDs of 5–30 s for the chosen data set showed no significant amplification by the surface layers, supporting the assumption that site effects were almost negligible (Fig. 3).

We used two measures of distance of the seismic stations from a fault plane and examined the variation in ground-motion predictions for both cases. One measure was the fault distance (FD), the shortest distance from the fault plane to a station (Campbell, 1981); the other was the equivalent hypocentral distance (EHD), the distance from a virtual point source that provides the same energy to the site as does a finite fault (Ohno *et al.*, 1993). EHD, which includes the effects of fault size, fault geometry, and inhomogeneous slip distribution, is defined as

$$X_{eq}^{-2} = \sum_{i=1}^{n} M_{0i}^2(f) X_i^{-2} \Big/ \sum_{i=1}^{n} M_{0i}^2(f), \tag{2}$$

in which n is the number of segments on the source fault; $M_{0i}(f)$ is the seismic moment on the ith segment (which is the product of rigidity, average slip over each segment of fault, and size of that segment); and X_i is the distance from the ith segment to a seismic station.

EHD values were calculated assuming uniform slip over the fault plane for most events except for the 2011 Tohoku earthquake, for which we used the heterogeneous slip distributions obtained by the inversion analysis of Y. Yokota *et al.* (2011). The data within a maximum FD were

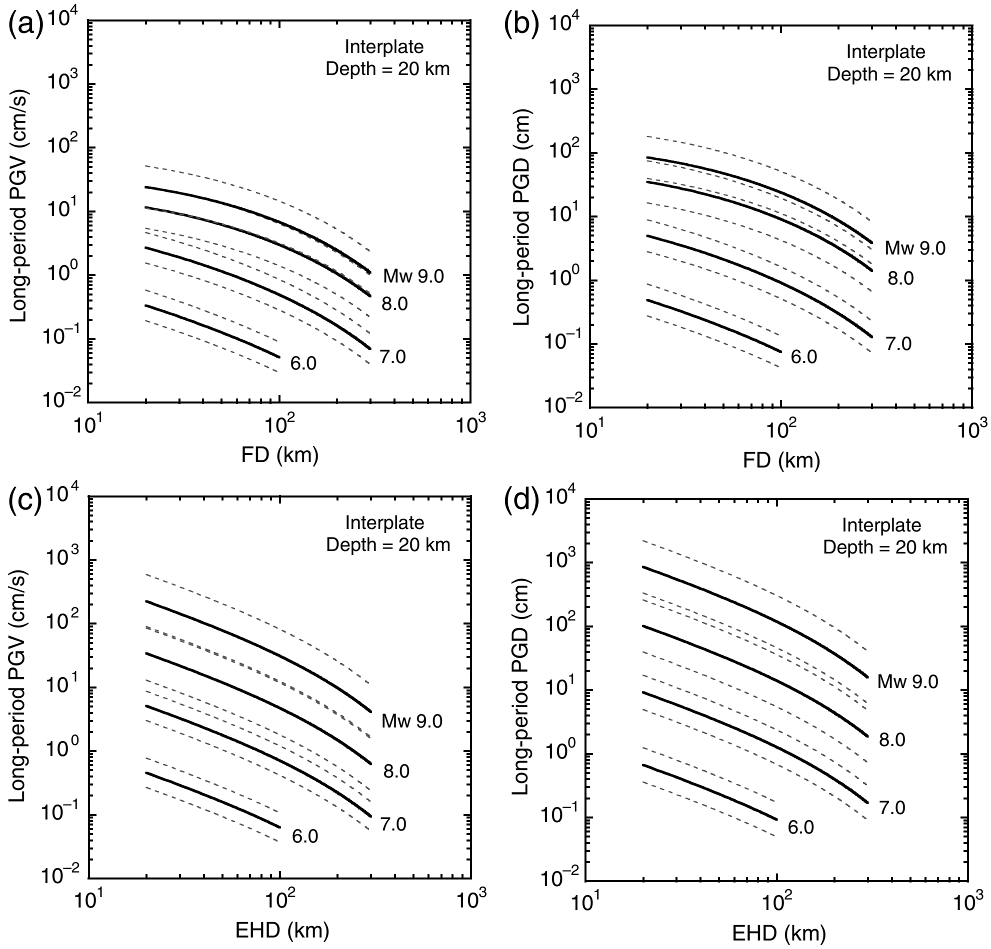

Figure 8. Long-period ground-motion prediction equations (GMPEs) of interplate earthquakes of M_w 6.0, 7.0, 8.0, and 9.0. The solid line denotes the mean value, and the two gray dashed lines denote ±sigma for long-period (a) PGVs versus FDs, (b) PGDs versus FDs, (c) PGVs versus EHDs, and (d) PGDs versus EHDs.

included, and the maximum FDs were defined as follows: 300 km for $M_w \geq 7$, 200 km for $6.4 < M_w < 7.0$, 150 km for $M_w = 6.4$, and 100 km for $M_w < 6.4$ (Fig. 4). We excluded the data with FD farther than the maximum FD to minimize the path effects of regression analysis. A total of 409 good-quality records from 103 stations were included in the final data set used to develop the long-period GMPEs. Most of the stations were located in the Honshu, Kyushu, and Shikoku regions; one station was located in the Hokkaido region (Fig. 1).

Table 2
Resultant Regression Coefficients a, h, d, and e and the Values of ε (i.e., the Standard Deviation of the Estimate)

					D				
Ground Motion	M_w	Distance Measure	*a*	*h*	Crustal	Interplate	Intraplate	*e*	ε
PGV	<7.5	FD	1.0061	0.0063	0.00	−0.6530	−0.5251	−4.5889	0.24
PGD	<7.5	FD	1.1099	0.0064	0.00	−0.6019	−0.5994	−5.0980	0.25
PGV	<7.5	EHD	1.0491	0.0047	0.00	−0.5844	−0.3964	−4.8037	0.23
PGD	<7.5	EHD	1.1382	0.0049	0.00	−0.5430	−0.4718	−5.2189	0.27
PGV	≥7.5	FD	0.3800	0.0063	0.00	−0.6530	−0.5251	0.2708	0.33
PGD	≥7.5	FD	0.4437	0.0064	0.00	−0.6019	−0.5994	0.1893	0.33
PGV	≥7.5	EHD	0.8174	0.0047	0.00	−0.5844	−0.3964	−3.1746	0.42
PGD	≥7.5	EHD	0.9277	0.0049	0.00	−0.5430	−0.4718	−3.6307	0.41

PGV, peak ground velocity and PGD, peak ground displacement.

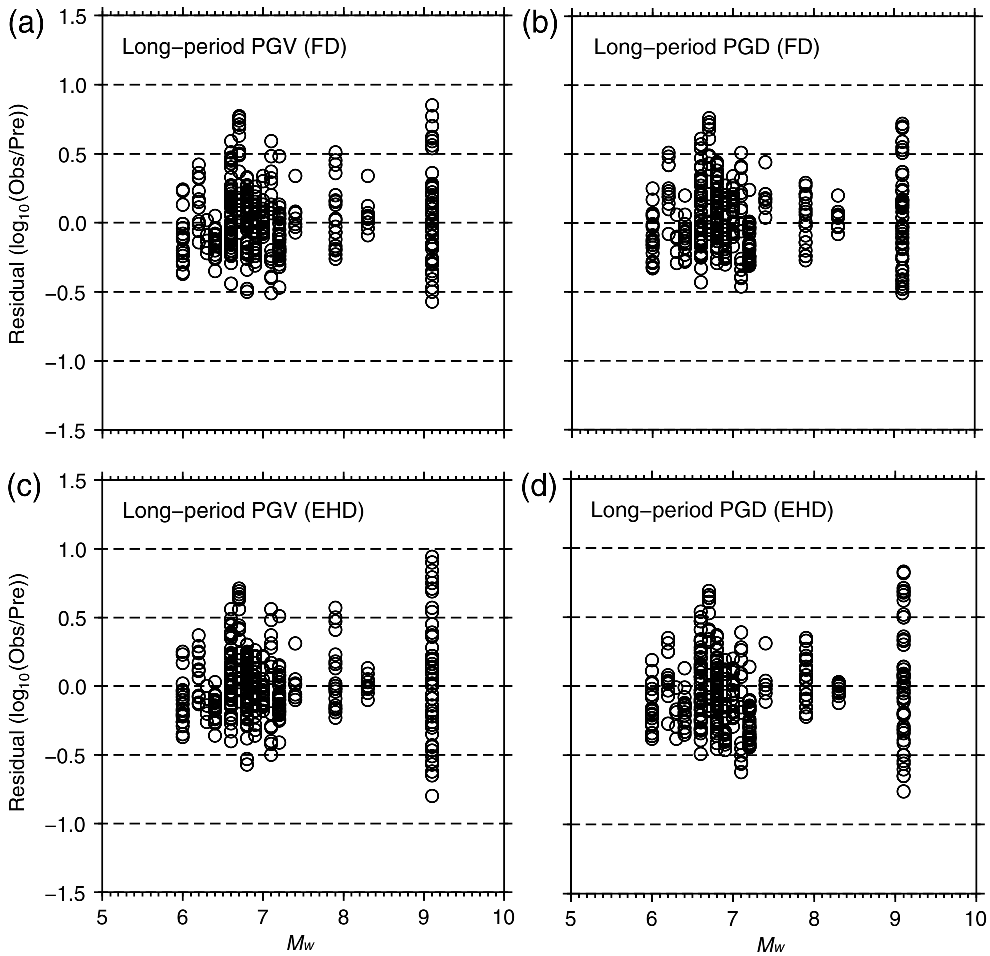

Figure 9. Distribution of residuals between observed (Obs) and predicted (Pre) long-period ground motions versus M_w for long-period (a) PGVs versus FDs, (b) PGDs versus FDs, (c) PGVs versus EHDs, and (d) PGDs versus EHDs.

Table 3
Standard Deviation ε after Second-Stage Regression Analyses Calculated for PGVs and FDs, PGDs and FDs, PGVs and EHDs, and PGDs and EHDs for Each Earthquake

				ε			
Number	Earthquake	Origin time (yyyy/mm/dd hh:mm)	M_w	PGV (FD)	PGD (FD)	PGV (EHD)	PGD (EHD)
1	Western Tottori	2000/10/06 13:30	6.7	0.47	0.46	0.43	0.41
2	Geiyo	2001/03/24 15:58	6.8	0.23	0.22	0.24	0.24
3	Miyagi-Oki	2002/11/03 12:37	6.4	0.18	0.19	0.20	0.25
4	Miyagi-Oki	2003/05/26 18:24	7.0	0.14	0.11	0.14	0.16
5	Northern Miyagi	2003/07/26 07:13	6.0	0.21	0.25	0.20	0.31
6	Tokachi-Oki	2003/09/26 04:50	8.3	0.12	0.07	0.07	0.06
7	Chuetsu	2004/10/23 17:56	6.6	0.14	0.18	0.15	0.19
8	Western Fukuoka	2005/03/20 10:53	6.6	0.33	0.36	0.31	0.32
9	Miyagi-Oki	2005/08/16 11:46	7.2	0.21	0.25	0.19	0.35
10	Chuetsu-Oki	2007/07/16 10:13	6.6	0.22	0.22	0.21	0.25
11	Ibaraki-Oki	2008/05/08 01:45	6.8	0.22	0.30	0.20	0.23
12	Iwate–Miyagi Nairiku	2008/06/14 08:43	6.9	0.17	0.18	0.18	0.26
13	Northern Iwate	2008/07/24 00:26	6.8	0.11	0.12	0.13	0.10
14	Suruga Bay	2009/08/11 05:07	6.2	0.21	0.32	0.17	0.22
15	Tohoku	2011/03/11 14:46	9.1	0.35	0.34	0.45	0.43
16	Iwate-Oki	2011/03/11 15:09	7.4	0.15	0.24	0.14	0.14
17	Ibaraki-Oki	2011/03/15 15:15	7.9	0.25	0.18	0.26	0.19
18	Northern Nagano	2011/03/12 03:59	6.3	0.18	0.21	0.20	0.28
19	Eastern Shizuoka	2011/03/15 22:31	6.0	0.24	0.22	0.24	0.26
20	Miyagi-Oki	2011/04/07 23:32	7.1	0.34	0.33	0.34	0.38

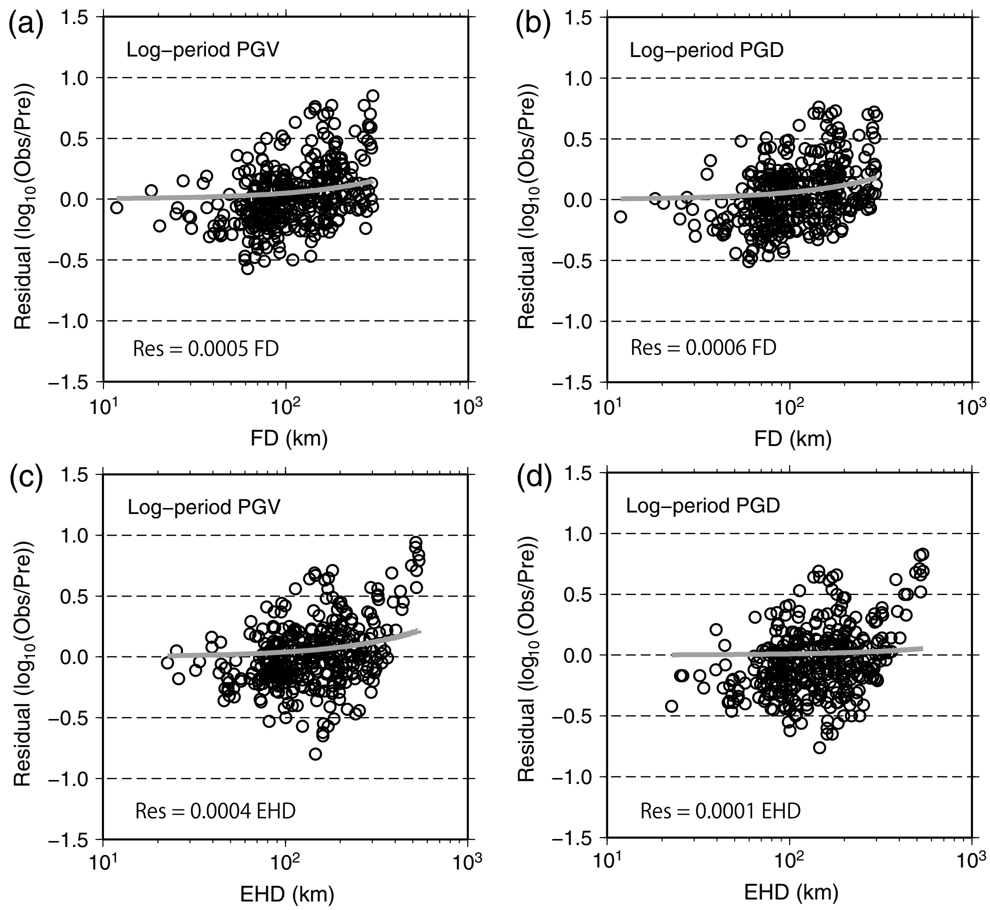

Figure 10. Distribution of residuals between observed (Obs) and predicted (Pre) long-period ground motions for long-period (a) PGVs versus FDs, (b) PGDs versus FDs, (c) PGVs versus EHDs, and (d) PGDs versus EHDs. The regressions (gray lines) show an increasing trend with distance; the corresponding equations are shown in each panel.

Development of Long-Period GMPEs

Regression Analysis

We used the regression models adopted by Si and Midorikawa (1999, 2000) for FD and EHD. The models are expressed as follows:

$$\log_{10} A = b - \log_{10}(X + c) - kX \tag{3}$$

and

$$\log_{10} A = b - \log_{10} X_{eq} - kX_{eq}, \tag{4}$$

in which A denotes PGV or PGD, X is FD in kilometers, and X_{eq} is EHD in kilometers. The first term on the right side of the equations (i.e., coefficient b) is magnitude dependent for each earthquake, the second term represents geometrical attenuation, and the third term represents anelastic attenuation ($k = 0.002$). Geometrical spreading of seismic waves causes geometrical attenuation, and anelastic attenuation is related to energy absorption caused by damping in the rocks (Schnabel and Seed, 1973).

For the case of FD, coefficient c was introduced to account for the saturation of A in the near-source area. In this study, we estimated the value of c using the following relation of Si and Midorikawa (1999, 2000):

$$c = 0.0028 \times 10^{0.5M_{\mathrm{w}}}. \tag{5}$$

For the case of the 2011 Tohoku earthquake, we used a value of $c = 39.55$ km, which corresponds to M_{w} 8.3, considering the strong ground motions saturate for earthquakes of $M_{\mathrm{w}} > 8.3$ (Si *et al.*, 2011).

We adopted a weighted regression to minimize bias related to the use of far-field data. We regressed those data according to their FD and EHD values. The weights were 8 for distances ≤25 km, 4 for distances of 25–50 km, 2 for distances of 50–100 km, and 1 for distances >100 km. Figure 5 shows the standard errors obtained using different weighting schemes for the 2000 western Tottori (M_{w} 6.7) and 2008 Iwate–Miyagi Nairiku crustal earthquakes. Standard errors were estimated between the observation and data

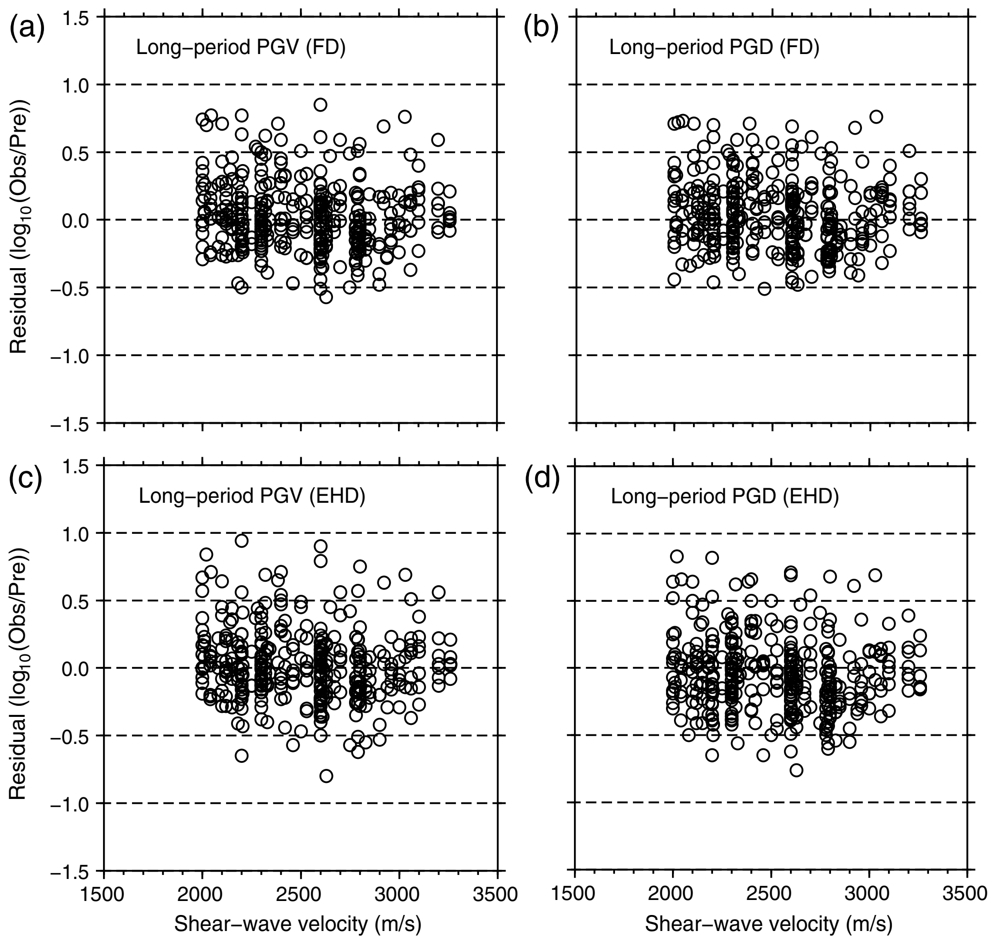

Figure 11. Distribution of residuals between observed (Obs) and predicted (Pre) long-period ground motions versus shear-wave velocity of the borehole bottom layer for long-period (a) PGVs versus FDs, (b) PGDs versus FDs, (c) PGVs versus EHDs, and (d) PGDs versus EHDs.

fits obtained using equations (3) and (4). The standard errors decreased and became progressively more stable with increasing weight. The weighting scheme used in this study appears to be reasonable to constrain near-field data and has a smaller effect on far-field data.

Regression analyses were performed on the final data set using the same two-stage regression analysis employed by Si and Midorikawa (1999, 2000). In the first stage, the regression models of equations (3) and (4) were fitted to the data in sequence, and coefficient b was determined for the long-period PGVs and PGDs of each earthquake with respect to the FDs and EHDs. In the second stage, the obtained values of b were plotted against M_w, as in Figure 6, which clearly shows that the scaling of coefficient b with M_w varies for large earthquakes of M_w 7.9, 8.3, and 9.1 compared to moderate earthquakes; that is, moderate earthquakes show strong scaling, whereas large earthquakes show weaker scaling. Because of this tendency, we set a hinge magnitude at $M_h = 7.5$ and proposed two separate relations for $M_w < 7.5$ and $M_w \geq 7.5$. Such a change in scaling with magnitude is probably period dependent; and, therefore, a larger value of M_h was selected by comparison with other studies that used short-period data (Boore *et al.*, 2014). We determined that the values of coefficient b exhibit less saturation with EHDs for $M_w \geq 7.5$ compared to FDs. However, a few data points deviated from the data fit. This deviation suggests other factors in addition to magnitude affect ground motion. Thus, we proposed using two additional factors, focal depth and earthquake type, to improve the quality of data fit while minimizing the observed variation. The proposed relation can be expressed as

$$b = aM_w + hD + \sum d_i S_i + e + \varepsilon, \qquad (6)$$

in which D is focal depth in kilometers; S_i is a dummy variable with a value of 1 for crustal, interplate, and intraplate earthquakes; ε is the standard deviation; and a, h, d_i, and e are regression coefficients. Although focal depth is implicitly included in the distance term X (i.e., the geometrical attenuation term) in equations (3) and (4), its inclusion in the magnitude-dependent term tightly constrains the source.

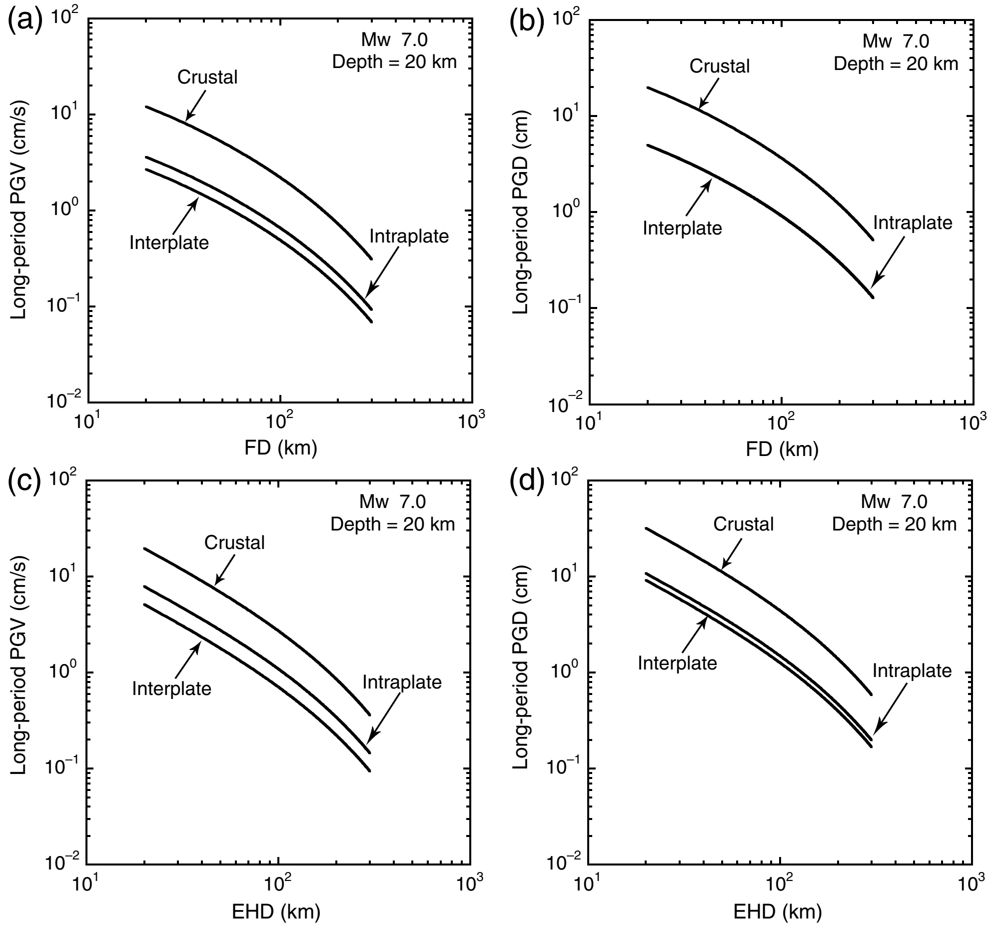

Figure 12. Long-period GMPEs of crustal, interplate, and intraplate earthquakes with a reference magnitude of M_w 7.0 and a reference depth of 20 km for long-period (a) PGVs versus FDs, (b) PGDs versus FDs, (c) PGVs versus EHDs, and (d) PGDs versus EHDs.

The effect of this term is significant, especially for deep events in which the source characteristics differ from those of shallow events (Wyss, 1970; Choy and Kirby, 2004). In the second-stage regression analysis, we first fitted $aM_w + e$ to the data to determine the values of coefficients a and e separately for earthquakes of $M_w < 7.5$ and $M_w \geq 7.5$. Then, the values of coefficients a and e were fixed in the regression analysis to determine the values of coefficients h and d_i. This analysis was only applied to earthquakes with $M_w < 7.5$. Because the number of earthquakes with $M_w \geq 7.5$ was insufficient to perform a full second-stage regression analysis, we adopted the values of h and d_i derived in the regression analysis for earthquakes with $M_w < 7.5$. The results of the regression analysis show that sufficiently small residuals were achieved for the value of coefficient b for individual earthquakes of $M_w < 7.5$ (Fig. 7).

Results and Discussion

Figure 8 shows our developed long-period GMPEs for crustal, interplate, and intraplate earthquakes of M_w 6.0, 7.0, 8.0, and 9.0 at 20 km depth. Table 2 lists the regression coefficients obtained in this study. The standard deviations for the cases in which long-period PGVs and PGDs are measured with respect to FDs and EHDs (Table 2) are very close for earthquakes of $M_w < 7.5$, implying that the different distance measures do not have much effect for earthquakes of $M_w < 7.5$. However, for earthquakes of $M_w \geq 7.5$, slightly larger standard deviations that were probably related to the 2011 Tohoku earthquake were observed when EHDs were used as the measure of distance compared with FDs, although few events showed smaller standard deviations corresponding to EHDs (Table 3). Nevertheless, we consider that the use of EHD as a measure of source–site distance is useful because it has a more physical basis than other distance measures (Douglas, 2003).

Figures 9–11 show the residuals of the observed and predicted long-period ground motions against M_w, distance, and shear-wave velocity at the bottom layer where the accelerometer is placed, respectively. The variability of observed-to-predicted long-period ground motion is larger for the value M_w 9.1, that of the 2011 Tohoku earthquake, which might be related to the event's huge source area. The residuals mostly fit the mean for near-field data at distances < 150 and < 300 km for FDs and EHDs, respectively; however, there is a trend in the

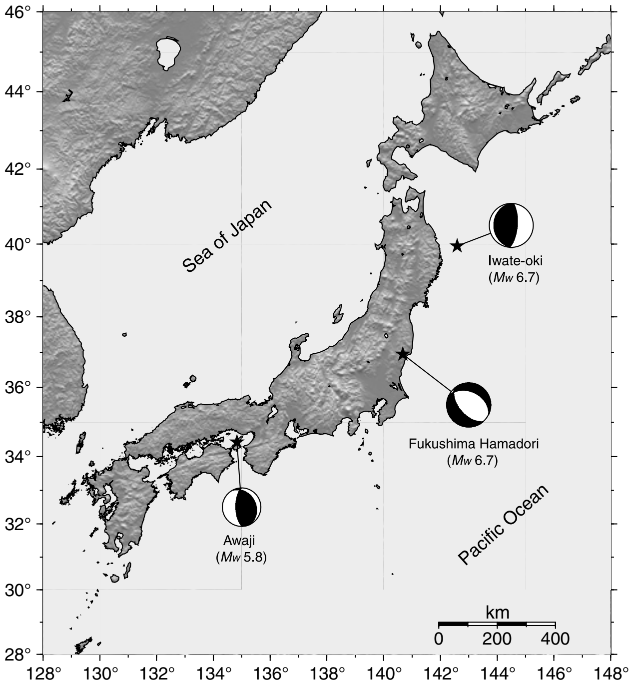

Figure 13. Epicenters (black stars) and focal mechanisms of the 2011 Fukushima Hamadori (M_w 6.7), 2011 Iwate-Oki (M_w 6.7), and 2013 Awaji (M_w 5.8) earthquakes. The focal mechanisms were obtained from the Global CMT project.

far-field data that could be caused by the dominant surface waves (Atkinson, 2004; Atkinson and Boore, 2006). To quantify the observed trend, we fitted the residuals using a linear regression considering the intercept at the mean of the near-field data. Thus, the fitting equation can be expressed as

$$\text{Res} = \log_{10}(\text{Obs}/\text{Pre}) = \alpha X, \tag{7}$$

in which Res is the residual; α is the regression coefficient, which has values of 0.0005, 0.0006, 0.0004, and 0.0001 for PGV-FD, PGD-FD, PGV-EHD, and PGD-EHD, respectively; and X is either FD or EHD. There is no apparent significant residual trend with shear-wave velocity of the bottom layer.

To assess the variability of long-period ground motion with earthquake type, we plotted the long-period GMPEs of PGVs and PGDs for crustal, interplate, and intraplate earthquakes (Fig. 12). We assumed a reference magnitude of M_w 7.0 and a depth of 20 km for the three earthquake types. The predicted long-period PGVs and PGDs of the crustal earthquake are larger than those of the interplate and intraplate earthquakes. To verify this, we selected two M_w 6.7 earthquakes: the 2011 Fukushima Hamadori earthquake with a focal depth of 6.4 km, which was a crustal earthquake (Hikima, 2012); and the 2011 Iwate-Oki earthquake with focal depth of 36 km, which was an interplate earthquake

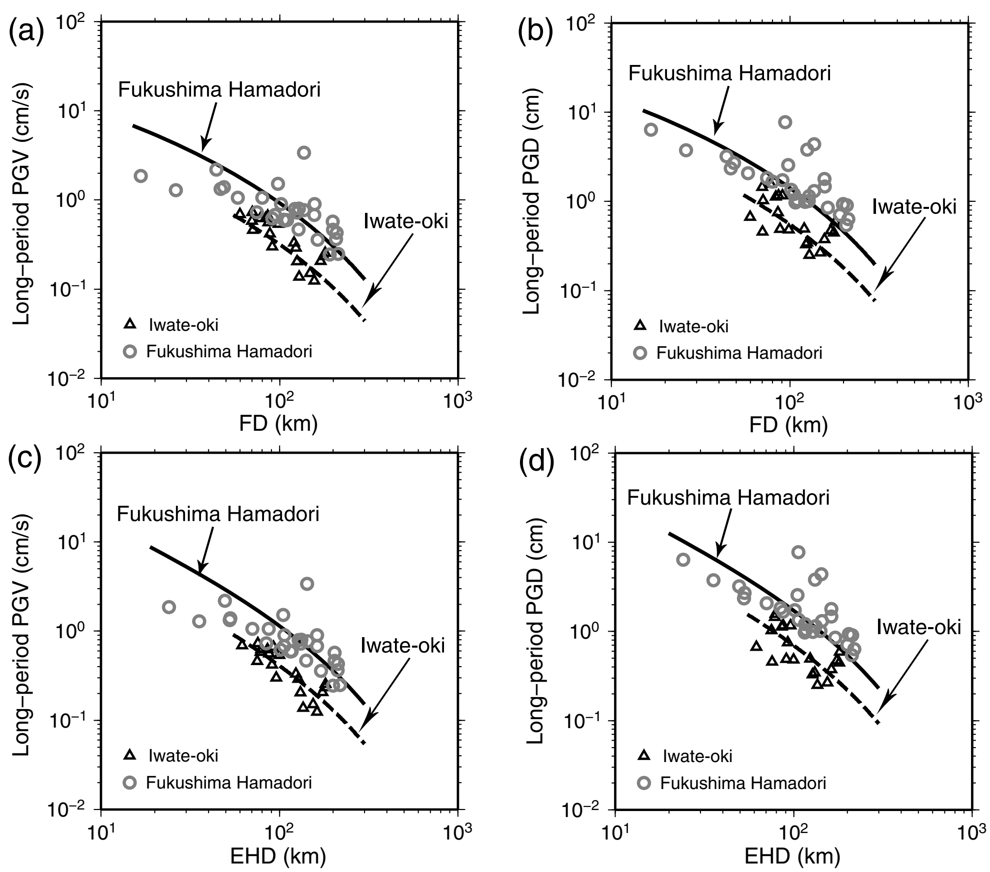

Figure 14. Comparison of long-period GMPEs and observed long-period (a, c) PGVs and (b, d) PGDs of a crustal earthquake (2011 Fukushima Hamadori, M_w 6.7) and an interplate earthquake (2011 Iwate-Oki, M_w 6.7).

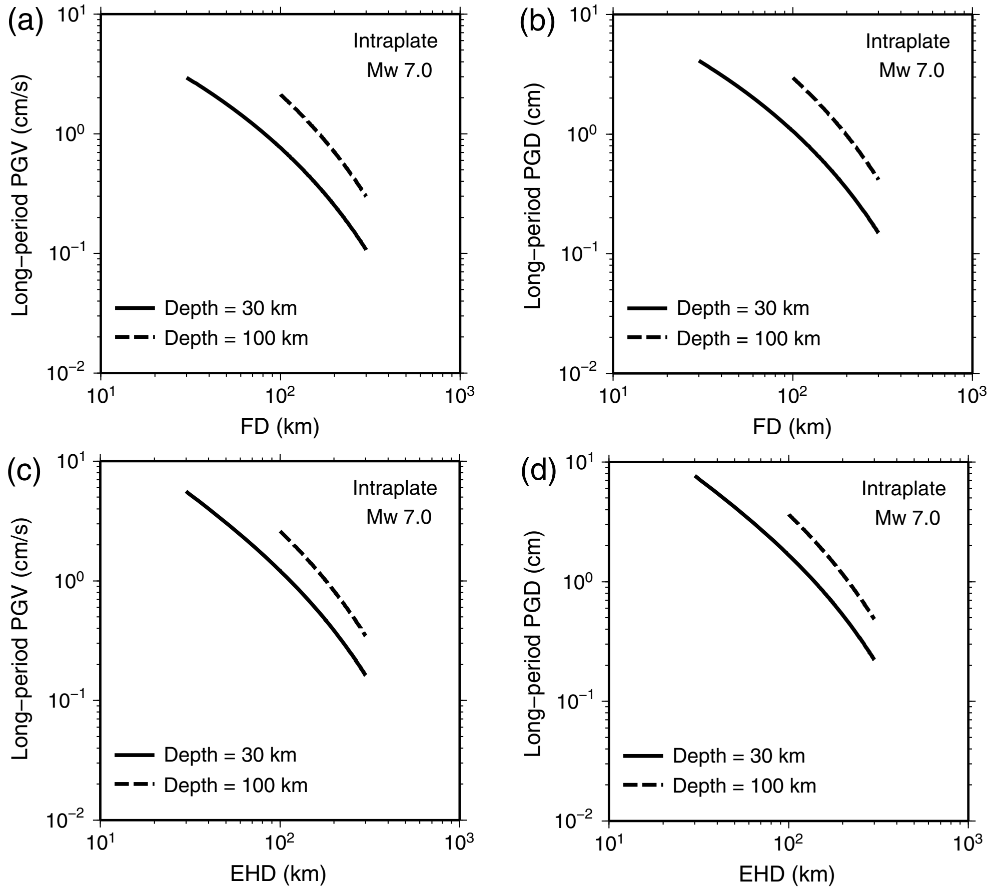

Figure 15. Long-period GMPEs of intraplate earthquakes with the same reference magnitude of M_w 7.0 and different depths of 30 and 100 km for long-period (a) PGVs versus FDs, (b) PGDs versus FDs, (c) PGVs versus EHDs, and (d) PGDs versus EHDs.

(Fig. 13). These two earthquakes were not included in the data set used for developing the long-period GMPEs. We filtered the strong-motion data of these two earthquakes in the 5–30 s range and integrated to obtain the long-period PGVs and PGDs as the vector summation of the two horizontal components. KiK-net borehole records with $V_S \geq 2000$ m/s were selected for comparison with the long-period GMPEs. Figure 14 shows that the observed and predicted long-period ground motions of the 2011 Fukushima Hamadori earthquake were larger than those of the 2011 Iwate-Oki earthquake. This finding may indicate the importance of the stress drop treatment in the GMPEs based on intraevent and interevent studies.

We also assessed the variability of the long-period ground motion with focal depth. We plotted the long-period GMPEs of PGVs and PGDs for two intraplate earthquakes of a reference magnitude of M_w 7.0 with differing depths of 30 and 100 km. The deeper earthquake produced larger ground motions than the shallower one (Fig. 15). We verified this finding with the 2001 Geiyo earthquake (M_w 6.8, 51 km depth) and the 2008 northern Iwate earthquake (M_w 6.8, 108 km depth). Figure 16 shows a comparison of the observed and predicted long-period PGVs and PGDs of those earthquakes. These results also confirm that both the observed and predicted long-period ground motions from the deeper earthquake are larger than those of the shallower earthquake. As the deepest earthquake in our data set (the 2008 northern Iwate earthquake) was located in the low-attenuation (high-Q) zone in northeast Japan (Utsu, 1967; Tsumura *et al.*, 2000); this could have caused less attenuation of the long-period ground motion in that region.

We compared our long-period GMPEs with the strong-motion data of the 2013 Awaji earthquake (M_w 5.8; see Fig. 13). The data recorded during this earthquake were not included in the data set used to derive the long-period GMPEs developed in this study; thus, those data can verify the validity of our long-period GMPEs. We collected data from 31 KiK-net downhole seismic stations located in hard-rock sites where $V_S \geq 2000$ m/s. The data were filtered using a band-pass filter of 5–30 s and integrated to obtain the long-period PGVs and PGDs. Subsequently, the maximum values of the vector summations of the two horizontal components were plotted against FDs and EHDs. We also plotted the predicted long-period GMPEs of this study (Fig. 17). From this, it is obvious that the

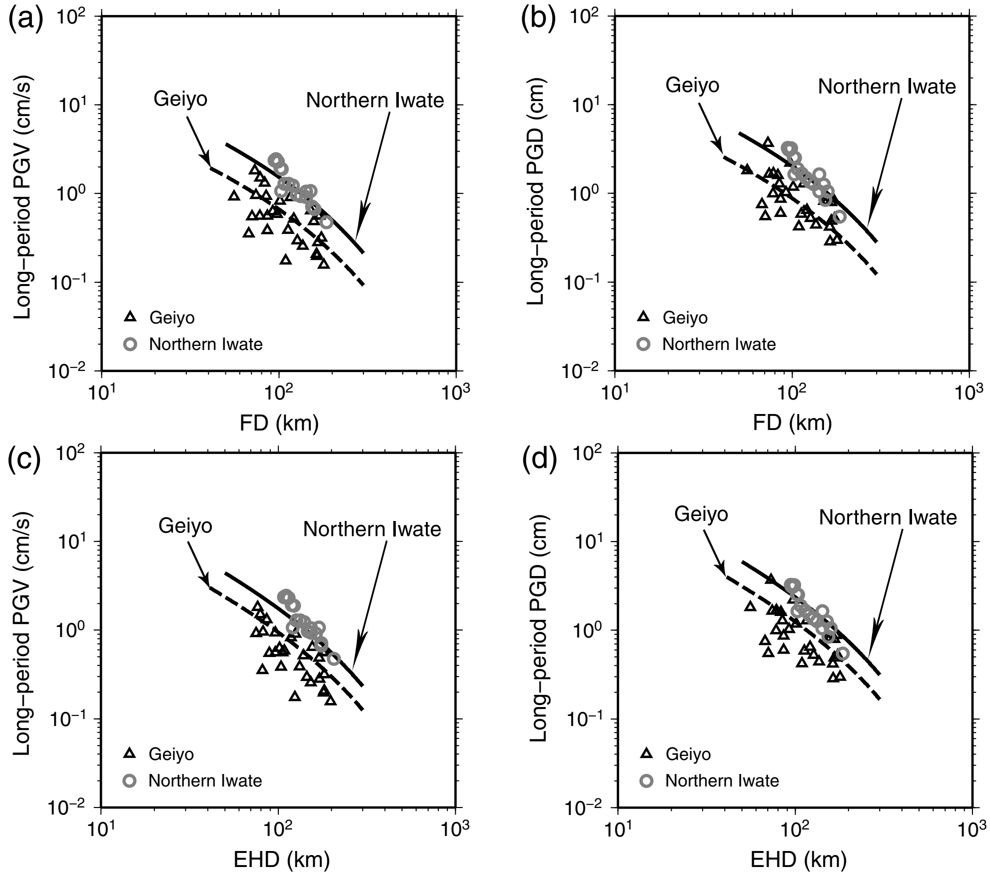

Figure 16. Comparison of long-period GMPEs and observed long-period (a, c) PGVs and (b, d) PGDs of two intraplate earthquakes with a reference magnitude of M_w 6.8 and different depths. The 2001 Geiyo earthquake had a focal depth of 51 km; the 2008 northern Iwate earthquake had a focal depth of 108 km.

observed and predicted long-period PGVs and PGDs are in good agreement.

Furthermore, we compared our estimated long-period GMPEs for PGDs with those of Campbell and Bozorgnia (2008), which were obtained with the GMRotI50 value of the two horizontal components (Boore *et al.*, 2006). Their model was developed for site conditions of $V_{S30} = 1100$ m/s, corresponding to class B (i.e., rock) of the National Earthquake Hazard Reduction Program of the Building Seismic Safety Council (BSSC, 2001), using strong-motion waveforms of 0.01–10 s. However, a comparison of that study with the results obtained in the present work might be valid, because PGDs are dominated by waveforms of long-period wavelength. Figure 18 compares these two models for three earthquakes with M_w of 6.0, 7.0, and 8.0. The comparison is limited to FD = 100 km for the M_w 6.0 earthquake and up to 200 km for the M_w 7.0 and 8.0 earthquakes, following the constraints of distance used in either study. The results of both studies are similar at distances up to 100 km; however, they differ slightly at distances >100 km. For example, the results of the study based on Japanese data showed relatively smaller PGDs than the results of Campbell and Bozorgnia (2008) based on the NGA database; this result may be related to regional differences in anelastic attenuation (Campbell and Bozorgnia, 2014).

Estimation of Moment Magnitude Based on Long-Period GMPEs

The observed data of a future earthquake can be modeled by equation (4) using EHDs as the measure of distance. The magnitude estimation requires the value of coefficient b, which can be obtained using an inversion technique. Following Molas and Yamazaki (1995), equation (4) can be expressed as

$$\mathbf{Y} = \mathbf{XB} + \boldsymbol{\epsilon}, \tag{8}$$

in which

$$\mathbf{Y} = \begin{bmatrix} \log A_1 \\ \log A_2 \\ \vdots \\ \log A_n \end{bmatrix}, \quad \mathbf{X} = \begin{bmatrix} 1 & \log X_1 & X_1 \\ 1 & \log X_2 & X_2 \\ \vdots & \vdots & \vdots \\ 1 & \log X_n & X_n \end{bmatrix},$$
$$\mathbf{B} = \begin{bmatrix} b \\ -1 \\ -0.002 \end{bmatrix}, \quad \text{and} \quad \boldsymbol{\epsilon} = \begin{bmatrix} \varepsilon_1 \\ \varepsilon_2 \\ \vdots \\ \varepsilon_n \end{bmatrix}. \tag{9}$$

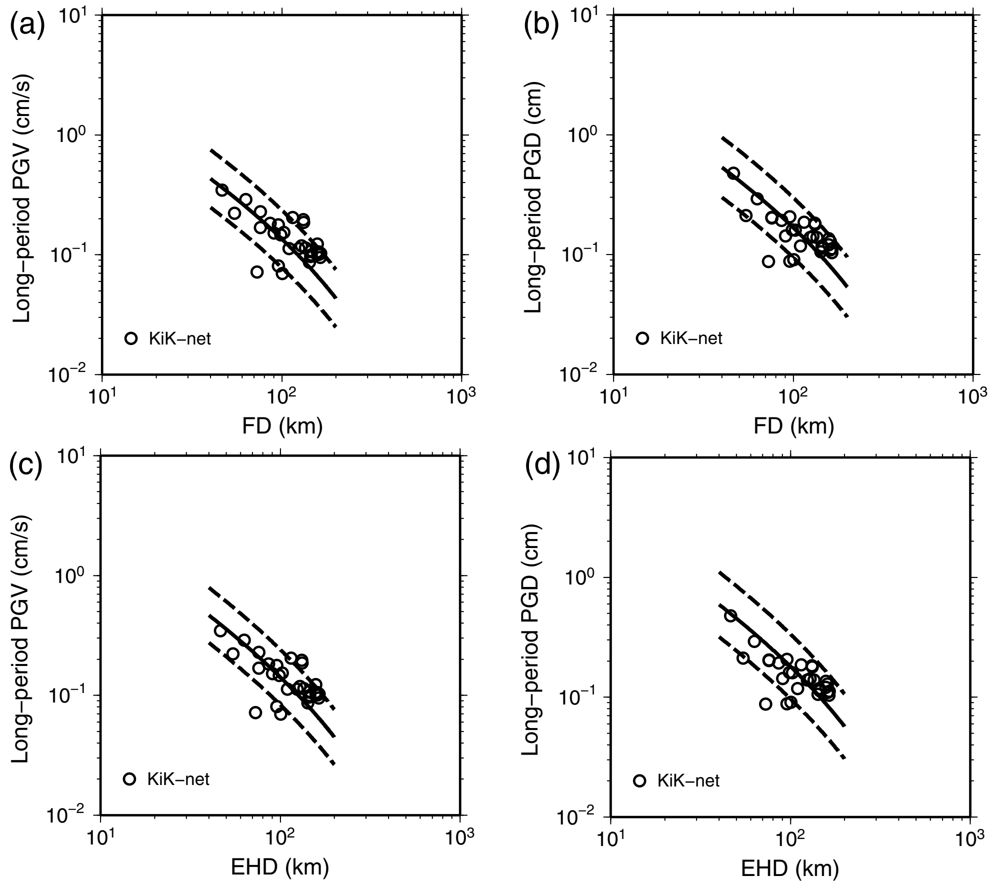

Figure 17. Comparison of long-period GMPEs and observed long-period ground motion for the 2013 Awaji earthquake (M_w 5.8) (solid line denotes the mean value, and the two dashed lines indicate ±sigma) for long-period (a) PGVs versus FDs, (b) PGDs versus FDs, (c) PGVs versus EHDs, and (d) PGDs versus EHDs.

The least-squares solution of equation (9) is

$$b = (X^T\mathbf{X})^{-1}X^T\mathbf{Y} + \boldsymbol{\epsilon}. \tag{10}$$

Because coefficient b is estimated from the data, the effects of earthquake type and focal depth are included in equation (10). Thus, M_w can be determined according to the following relation:

$$M_w = (b - hD - \sum d_i S_i - e)/a. \tag{11}$$

Because the term $\mathbf{X} + c$ in equation (3) is also a function of M_w, it is not easy to use the previously proposed least-squares method to estimate M_w for the GMPEs obtained with FDs; therefore, we proposed a grid-search method to overcome this problem. With this method, the best solution for the magnitude is obtained by varying M_w to minimize the root mean square error (rmse) between the observed and predicted long-period PGVs or PGDs, as follows:

$$\mathrm{rmse} = \sqrt{\frac{\sum_{i=1}^{n}(X_{\mathrm{obs}} - X_{\mathrm{pred}})^2}{n}}, \tag{12}$$

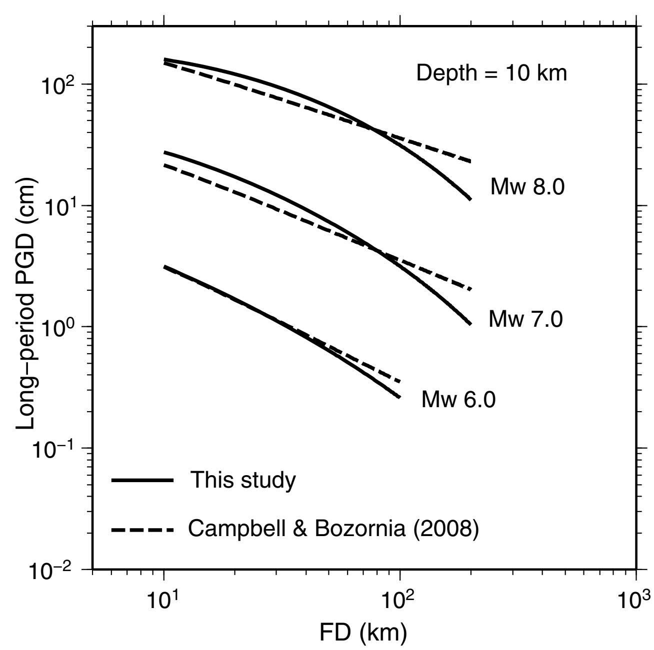

Figure 18. Comparison of the GMPEs in this study and those obtained by Campbell and Bozorgnia (2008) for earthquakes of M_w 6.0, 7.0, and 8.0. We used a reference focal depth of 10 km for the three earthquakes.

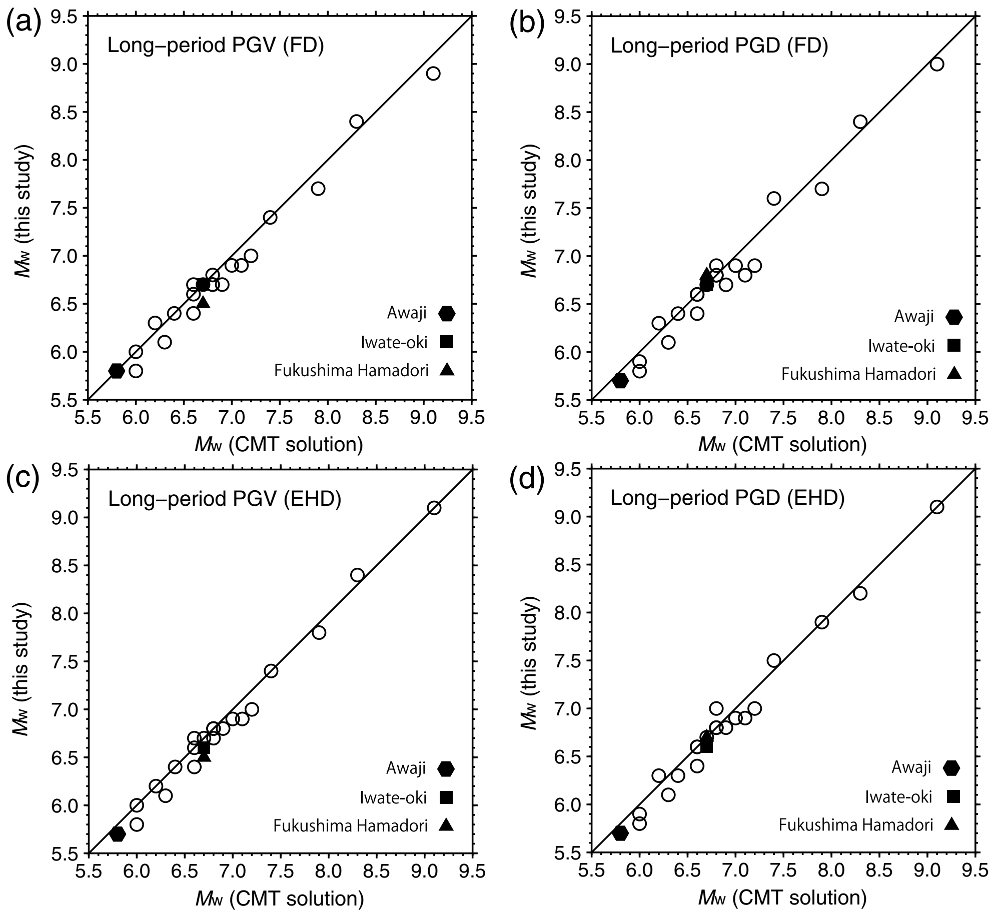

Figure 19. Comparison between our M_w estimates and those obtained from the Global CMT project for long-period (a) PGVs versus FDs, (b) PGDs versus FDs, (c) PGVs versus EHDs, and (d) PGDs versus EHDs. We plotted the (1:1) line for comparison. Black circles denote the earthquakes used to develop the long-period GMPEs, triangles the 2011 Fukushima Hamadori earthquake, squares the 2011 Iwate-Oki earthquake, and hexagons the 2013 Awaji earthquake.

in which X_{obs} is the observed strong ground motion, X_{pred} is the predicted value obtained from the long-period GMPEs, and n is the total number of records.

We applied these methods to estimate the moment magnitude of the 20 earthquakes used in the development of the long-period GMPEs. In addition, we estimated the moment magnitude of the 2011 Fukushima Hamadori, 2011 Iwate-Oki, and 2013 Awaji earthquakes. The estimates were made based on the observed KiK-net borehole strong-motion data. Correction of the residual trend (i.e., equation 7) was applied to the data set used to estimate the magnitude. Table 4 lists the values of error calculated as the difference between the values of M_w obtained in this study and those of the Global CMT project. Figure 19 compares the values of M_w of this study and those of the Global CMT project. These comparisons reveal (1) the predictions of M_w based on our estimates are generally similar to those of the Global CMT project, within error limits of ± 0.2; (2) there is good agreement between the two estimates for large earthquakes with errors mainly distributed within ± 0.1; and (3) the results based on EHDs are slightly better than those based on FDs, as inferred from the low values of the standard errors.

The method proposed here, which requires information about the seismic fault (i.e., fault geometry and hypocenter depth) is based on a simple calculation that could be computed a short time after the occurrence of a disastrous earthquake. Based on a preassumed fault model, Ibrahim (2013) and Ibrahim *et al.* (2014) proposed a method for rapidly estimating the value of M_w of interplate earthquakes. That method is based on calculating FD from different-size fault planes centered at the hypocenter location that is quickly available from JMA, where the source dimensions (i.e., fault length and width) are estimated based on empirical scaling relations (e.g., Blaser *et al.*, 2010). The magnitude estimate is finally obtained from the appropriate fault model with the smallest error.

Conclusions

We established long-period GMPEs of band-pass-filtered PGVs and PGDs of 5–30 s based on NIED/KiK-net borehole

Table 4
Estimates of Moment Magnitudes and Their Errors with Respect to the Global Centroid Moment Tensor (CMT) Project

Number	Earthquake	M_w (CMT)	M_w (PGV−FD)	Error	M_w (PGDVFD)	Error	M_w (PGV−EHD)	Error	M_w (PGD−EHD)	Error
1	Western Tottori	6.7	6.9	0.2	6.9	0.2	6.9	0.2	6.8	0.1
2	Geiyo	6.8	6.9	0.1	7.0	0.2	6.9	0.1	7.0	0.2
3	Miyagi-Oki	6.4	6.3	−0.1	6.3	−0.1	6.2	−0.2	6.3	−0.1
4	Miyagi-Oki	7.0	7.0	0	7.0	0	6.9	−0.1	7.0	0
5	Northern Miyagi	6.0	5.9	−0.1	5.8	−0.2	5.9	−0.1	5.9	−0.1
6	Tokachi-Oki	8.3	8.5	0.2	8.4	0.1	8.3	0	8.3	0
7	Chuetsu	6.6	6.5	−0.1	6.6	0	6.6	0	6.6	0
8	Western Fukuoka	6.6	6.7	0.1	6.7	0.1	6.7	0.1	6.7	0
9	Miyagi-Oki	7.2	7.1	−0.1	7.0	−0.2	7.1	−0.1	7.1	−0.1
10	Chuetsu-Oki	6.6	6.5	−0.1	6.5	−0.1	6.5	−0.1	6.5	−0.1
11	Ibaraki-Oki	6.8	6.7	−0.1	6.8	0	6.7	−0.1	6.8	0
12	Iwate–Miyagi Nairiku	6.9	6.8	−0.1	6.8	−0.1	6.8	−0.1	6.8	−0.1
13	Northern Iwate	6.8	6.9	0.1	6.9	0.1	6.9	0.1	6.9	0.1
14	Suruga Bay	6.2	6.3	0.1	6.4	0.2	6.3	0.1	6.3	0.1
15	Tohoku	9.1	9.1	0	9.1	0	9.2	0.1	9.1	0
16	Iwate-Oki	7.4	7.4	0	7.7	0.3	7.4	0	7.6	0.2
17	Ibaraki-Oki	7.9	8.0	0.1	7.9	0	8.0	0.1	7.9	0
18	Northern Nagano	6.3	6.1	−0.2	6.1	−0.2	6.1	−0.2	6.1	−0.2
19	Eastern Shizuoka	6.0	5.8	−0.2	5.9	−0.1	5.8	−0.2	5.9	−0.1
20	Miyagi-Oki	7.1	7.0	−0.1	7.0	−0.1	7.1	0	7.1	0
21	Fukushima Hamadori	6.7	6.5	−0.2	6.8	0.1	6.5	−0.2	6.7	0
22	Iwate-Oki	6.7	6.5	0.2	6.6	−0.1	6.4	−0.3	6.5	−0.2
23	Awaji	5.8	5.8	0.0	5.8	0.0	5.8	0.0	5.7	−0.1
	Error (Maximum)			0.2	—	0.2	—	0.3	—	0.2
	Standard deviation (σ)			0.12		0.15		0.12		0.11

strong-motion data. The long-period GMPEs predict the ground motion for bedrock of $V_S \geq 2000$ m/s. The developed GMPEs suggested a bilinear relation bended at M_w 7.5, compensating for the effects of corner frequency and avoiding saturation at large magnitudes.

We studied the variability of the predicted long-period ground motion for two different measures of distance: FDs and EHDs. We determined that uncertainty decreases when using FDs rather than EHDs for earthquakes of $M_w \geq 7.5$. Our long-period GMPEs predicted larger ground motions from crustal earthquakes than from interplate or intraplate earthquakes and indicated that long-period PGVs and PGDs increase with increasing focal depth.

The developed long-period GMPEs were used to estimate the moment magnitude: the values of M_w calculated by our method are consistent with those obtained by the Global CMT project. The proposed method uses strong-motion data from close stations for which the entire record can be obtained within a few minutes of the earthquake origin time. The method was proven to be useful for estimating the moment magnitude of great earthquakes such as the 2011 Tohoku earthquake. Moment magnitude estimation can be rapidly achieved if information such as the fault geometry and focal depth are available. The main advantages of our method for moment magnitude estimation in comparison with other traditional magnitude scales such as M_s and M_{JMA} are (1) M_w estimates are based on the long-period GMPEs established on hard-rock sites and, therefore, site effects are almost negligible and (2) M_w estimates will not be saturated, even for great earthquakes.

In addition to the above-mentioned application to moment magnitude estimations, our developed long-period GMPEs will provide useful information for engineering applications and hazard assessment of structures with predominant periods of 5–30 s.

Data and Resources

The strong-motion data and borehole information are available via the KiK-net website, National Institute of Earth Science and Disaster Prevention at http://www.kyoshin.bosai.go.jp/kyoshin/search/index_en.html (last accessed November 2015). The hypocenter locations of the data set are as stated in the Japan Meteorological Agency (JMA) unified catalog. The M_w values of the data set were obtained from the Global Centroid Moment Tensor (CMT) project catalog (http://www.globalcmt.org/CMTsearch.html, last accessed November 2015). The source model information of the 2002 Miyagi-Oki (M_w 6.4) earthquake was obtained from the Earthquake Information Center (EIC) Seismological Note Number 128 (http://wwweic.eri.u-tokyo.ac.jp/sanchu/Seismo_Note/index-e.html, last accessed November 2015). The source model information of the 2011 Iwate-Oki (M_w 7.4), 2011 Eastern Shizouka (M_w 6.0), 2011 Miyagi-Oki (M_w 6.0), 2011 Iwate-Oki (M_w 6.7), and 2013 Awaji (M_w 5.8) earthquakes were obtained from the JMA (http://www.data.jma.go.jp/svd/eqev/data/sourceprocess/index.html, last accessed November 2015).

Acknowledgments

We acknowledge Ezio Faccioli, Richard Lee, and Peter J. Stafford for thoughtful comments. We thank Kazuhito Hikima for providing us the source model information of the 2011 Fukushima Hamadori earthquake.

References

Abrahamson, N., and W. Silva (2008). Summary of the Abrahamson & Silva NGA ground-motion relations, *Earthq. Spectra* **24,** 67–97.

Abrahamson, N., W. Silva, and R. Kamai (2014). Summary of ASK14 ground-motion relation for active crustal regions, *Earthq. Spectra* **30,** 1025–1055.

Aoi, S., T. Kunugi, and H. Fujiwara (2004). Strong-motion seismograph network operated by NIED: K-NET and KiK-net, *J. Japan Assoc. Earthq. Eng.* **4,** no. 3, 65–74.

Aoi, S., H. Sekiguchi, R. Honda, N. Morikawa, T. Kunugi, and H. Fujiwara (2003). Ground motion and rupture process of the 26 May 2003 Off-Miyagi earthquake obtained from strong motion data of K-NET and KiK-net, *Programme and Abstract of Seismol. Soc. Japan*, Kyoto, Japan, 6–8 October 2003, Abstract A077 (in Japanese).

Asano, K., and T. Iwata (2006). Source process and near-source ground motions of the 2005 West Off Fukuoka Prefecture earthquake, *Earth Planets Space* **58,** 93–98.

Atkinson, G. M. (2004). Empirical attenuation of ground-motion spectral amplitudes in southeastern Canada and northeastern United States, *Bull. Seismol. Soc. Am.* **94,** 1079–1095.

Atkinson, G. M., and D. M. Boore (2006). Earthquake ground-motion prediction equations for eastern North America, *Bull. Seismol. Soc. Am.* **96,** 2181–2205.

Blaser, L., K. Frank, M. Ohrnberger, and F. Scherbaum (2010). Scaling relations of earthquake source parameter estimates with special focus on subduction environment, *Bull. Seismol. Soc. Am.* **100,** 2914–2926.

Boore, D. M (2005). Long-period ground motions from digital acceleration recordings: A new era in engineering seismology, in *Directions in Strong Motion Instrumentation*, P. Gülkan and J. G. Anderson (Editors), Springer, Dordrecht, The Netherlands, 41–54.

Boore, D. M., and G. M. Atkinson (2008). Ground-motion prediction equations for the average horizontal component of PGA, PGV, and 5%-damped PSA at spectral periods between 0.01 s and 10.0 s, *Earthq. Spectra* **24,** 99–138.

Boore, D. M., J. P. Stewart, E. Seyhan, and G. M. Atkinson (2014). NGA-West 2 equations for predicting PGA, PGV, and 5%-damped PSA for shallow crustal earthquakes, *Earthq. Spectra* **30,** 1057–1085.

Boore, D. M., J. Waston-Lamprey, and N. A. Abrahamson (2006). Orientation-independent measures of ground motion, *Bull. Seismol. Soc. Am.* **96,** 1502–1511.

Building Seismic Safety Council (BSSC) (2001). NEHRP recommended provisions for seismic regulations for new buildings and other structures (FEMA 368), 2000 Edition, Part 1: Provisions, prepared by the Building Seismic Safety Council for the Federal Emergency Management Agency, Washington, D.C., 374 pp.

Campbell, W. K. (1981). Near-source attenuation of peak horizontal acceleration, *Bull. Seismol. Soc. Am.* **71,** 2039–2070.

Campbell, W. K., and Y. Bozorgnia (2008). NGA ground motion model for the geometric mean horizontal component of PGA, PGV, PGD and 5% damped linear elastic response spectra for periods ranging from 0.01 to 10 s, *Earthq. Spectra* **24,** 139–171.

Campbell, W. K., and Y. Bozorgnia (2014). NGA-West2 ground motion model for the average horizontal components for PGA, PGV, and 5%-damped linear acceleration response spectra, *Earthq. Spectra* **30,** 1087–1115.

Chiou, S.-J. B., and R. Youngs (2008). An NGA model for the average horizontal component of peak ground motion and response spectra, *Earthq. Spectra* **24,** 173–215.

Chiou, S.-J. B., and R. Youngs (2014). Update of the Chiou and Youngs NGA model for the average horizontal component of peak ground motion and response spectra, *Earthq. Spectra* **30,** 1117–1153.

Choy, G. L., and S. H. Kirby (2004). Apparent stress, fault maturity and seismic hazard for normal-fault earthquakes at subduction zones, *Geophys. J. Int.* **159,** 991–1012.

Dhakal, Y. P., T. Kunugi, W. Suzuki, and S. Aoi (2013). Attenuation relation of absolute velocity response spectra (1-10 s) in Japan: A preliminary analysis, *Proc. 2nd Int. Symp. Earthq. Eng., JAEE*, Tokyo, Japan, 11–12 November 2013, 39–48.

Douglas, J. (2003). Earthquake ground motion estimation using strong-motion records: A review of equations for the estimation of peak ground acceleration and response spectral ordinates, *Earth Sci. Rev.* **61,** 43–104.

Dziewonski, A. M., T.-A. Chou, and J. H. House (1981). Determination of earthquake source parameters from waveform data for studies of global and regional seismicity, *J. Geophys. Res.* **86,** 2825–2852.

Gutenberg, B. (1945). Amplitudes of surface waves and magnitudes of shallow earthquakes, *Bull. Seismol. Soc. Am.* **35,** 3–12.

Hanks, T. C. (1976). Observations and estimation of long-period strong ground motion in Los Angeles basin, *Earthq. Eng. Struct. Dyn.* **4,** 473–488.

Hanks, T. C., and H. Kanamori (1979). A moment magnitude scale, *J. Geophys. Res.* **82,** 2981–2987.

Hayes, P. G., P. S. Earle, H. M. Benz, D. J. Wald, R. W. Briggs, and the USGS/NEIC Earthquake Response Team (2011). 88 Hours: The U.S. Geological Survey National Earthquake Information Center response to the 11 March 2011 M_w 9.0 Tohoku earthquake, *Seismol. Res. Lett.* **82,** 481–493.

Heaton, T., F. Tajima, and A. W. Mori (1986). Estimating ground motions using recorded accelerograms, *Surv. Geophys.* **8,** 25–83.

Hikima, K. (2012). Rupture process of the April 11, 2011 Fukushima Hamadori earthquake (M_j 7.0), *Zisin* **64,** 234–256 (in Japanese with English abstract).

Hikima, K., and K. Koketsu (2004). Source processes of the foreshock, mainshock and largest aftershock in the 2003 Miyagi-ken Hokubu, Japan, earthquake sequence, *Earth Planets Space* **56,** 87–93.

Horikawa, H. (2005). A fault model of the 2004 Mid Niigata (Chuestu) earthquake deduced from strong motion records and relocated hypocenters, *Jpn. Geosci. Union Meet.*, Abstract S079–P004.

Ibrahim, R. (2013). Long-period ground motion prediction equations and their application to the magnitude estimation of large earthquakes considering site effects, *Ph.D. Thesis*, University of Tokyo, Japan, 294 pp.

Ibrahim, R., H. Si, K. Koketsu, and H. Miyake (2014). Moment magnitude estimate of large earthquakes based on long-period ground motion prediction equations and pre-assumed fault models, *Proc. of the 14th Japan Earthquake Engineering Symposium*, Tokyo, Japan, 4–6 December 2014, 595–603.

Idriss, M. (2008). An NGA empirical model for estimating the horizontal spectral values generated by shallow crustal earthquakes, *Earthq. Spectra* **24,** 217–242.

Idriss, M. (2014). An NGA-West2 empirical model for estimating the horizontal spectral values generated by shallow crustal earthquakes, *Earthq. Spectra* **30,** 1155–1177.

Irikura, K. (2008). Lesson from the 2007 Niigata-ken Chuestu-Oki earthquake on seismic safety for nuclear power plant, *Bull. Japan Assoc. Earthq. Eng.* **7,** 25–29 (in Japanese).

Iwata, T., and H. Sekiguchi (2002). Source process of the 2000 western Tottori earthquake and source strong motions in the epicentral area, *Chikyu Monthly* **38,** 182–188 (in Japanese).

Kanamori, H. (1977). The energy release in great earthquakes, *J. Geophys. Res.* **82,** 2981–2987.

Kanamori, H. (1979). A semi-empirical approach to prediction of long-period ground motions from great earthquakes, *Bull. Seismol. Soc. Am.* **69,** 1645–880.

Kanamori, H., and L. Rivera (2008). Source inversion of *W* phase: Speeding up seismic tsunami warning, *Geophys. J. Int.* **175,** 222–238.

Kataoka, S., S. Matsumoto, T. Kusakabe, and N. Toyama (2008). Attenuation relationships and amplification map for ground motion in rather-long period range, *J. Japan Soc. Civil Eng.* **64,** 721–738 (in Japanese with English abstract).

Katsumata, A. (1996). Comparison of magnitudes estimated by the Japan Meteorological Agency with moment magnitudes for intermediate and deep earthquakes, *Bull. Seismol. Soc. Am.* **86,** 832–842.

Kinoshita, S. (1998). Kyoshin Net (K-NET), *Seismol. Res. Lett.* **69,** 309–332.

Koketsu, K., and H. Miyake (2008). A seismological overview of long-period ground motion, *J. Seismol.* **12,** 133–143.

Koketsu, K., K. Hikima, S. Miyazaki, and S. Ide (2004). Joint inversion of strong motion and geodetic data for the 2003 Tokachi-Oki, Hokkaido, earthquake, *Earth Planets Space* **56,** 329–334.

Molas, G. L., and F. Yamazaki (1995). Attenuation of earthquake ground motion in Japan including deep focus events, *Bull. Seismol. Soc. Am.* **85,** 1343–1358.

Ohno, S., T. Ohta, T. Ikeura, and M. Takemura (1993). Revision of attenuation formula considering the effect of fault size to evaluate strong motion spectra in near field, *Tectonophysics* **218,** 69–81.

Ohta, Y., T. Kobayashi, H. Tsushima, S. Miura, R. Hino, T. Takasu, H. Fujimoto, T. Iinuma, K. Tachibana, T. Demachi, *et al.* (2012). Quasi real-time fault model estimation for near-field tsunami forecasting based on RTK-GPS analysis: Application to the 2011 Tohoku-Oki earthquake (M_w 9.0), *J. Geophys. Res.* **117,** 1–16.

Paolucci, R., A. Rovelli, E. Faccioli, C. Cauzzi, D. Finazzi, M. Vanini, C. Di Alessandro, and G. Calderoni (2008). On the reality of long-period response spectral ordinates from digital accelerograms, *Earthq. Eng. Struct. Dyn.* **37,** 697–710.

Purcaru, G., and H. Berckhemer (1978). A magnitude scale for very large earthquakes, *Tectonophysics* **49,** 189–198.

Research Center for Seismology, Volcanology and Disaster Mitigation, Graduate School of Environmental Studies, Nagoya University (2008). Source process of Off-Ibaraki earthquake on May 8, 2008 (M_j 6.4, 7.0), *Report of the Coordinating Committee for Earthquake Prediction*, Vol. **80,** 108–110 (in Japanese).

Schnabel, P. B., and H. B. Seed (1973). Accelerations in rock for earthquakes in the western United States, *Bull. Seismol. Soc. Am.* **63,** 501–516.

Si, H., and S. Midorikawa (1999). New attenuation relationship for peak ground acceleration and velocity considering effects of fault type and site condition, *J. Struct. Constr. Eng., AIJ* **523,** 63–70 (in Japanese with English abstract).

Si, H., and S. Midorikawa (2000). New attenuation relationship for peak ground acceleration and velocity considering effects of fault type and site condition, *Proc. 12th World Conf. Earthq. Eng.*, Auckland, New Zealand, 30 January–4 February 2000, Paper Number 0532.

Si, H., H. S. Kuyuk, K. Koketsu, and H. Miyake (2011). Attenuation characteristics of peak ground motion during the 2011 Tohoku earthquake, Japan, earthquake, *Seismol. Res. Lett.* **82,** 460.

Somerville, P., and R. Graves (1993). Conditions that give rise to usually large long period ground motions, *Structural Design of Tall Buildings* **2,** 211–232.

Suzuki, W., and S. Aoi (2009). Rupture process of the 2009 Suruga-Bay earthquake derived from near-source strong-motion records, *Report of the Coordinating Committee for Earthquake Prediction*, Vol. **83,** 259–262 (in Japanese).

Suzuki, W., S. Aoi, and H. Sekiguchi (2009). Rupture process of the 2008 northern Iwate intraslab earthquake derived from near-source strong-motion records, *Bull. Seismol. Soc. Am.* **99,** 2825–2835.

Suzuki, W., S. Aoi, and H. Sekiguchi (2010). Rupture process of the 2008 Iwate-Miyagi Nairiku, Japan, earthquake derived from near-source strong-motion records, *Bull. Seismol. Soc. Am.* **100,** 256–266.

Takeda, T. (2011). The earthquake in the vicinity of Nagano and Niigata Prefecture boundary on March 12, 2011, *Report of the Coordinating Committee for Earthquake Prediction*, Vol. **86,** 486–487 (in Japanese).

Tsumura, N., S. Matsumoto, S. Horiuchi, and A. Hasegawa (2000). Three-dimensional attenuation structure beneath the northeastern Japan arc estimated from spectra of small earthquakes, *Tectonophysics* **319,** 241–260.

Utsu, T. (1967). Anomalies in seismic wave velocity and attenuation associated with a deep earthquake zone (I), *J. Fac. Sci. Hokkaido Univ. Ser. VII* **3,** 1–25.

Wang, G-Q., D. M. Boore, G. Tang, and X. Zhou (2007). Comparisons of ground motions from colocated and closely spaced one-sample-per second global positioning system and accelerograph recordings of the 2003 M 6.5 San Simeon, California, earthquake in Parkfield region, *Bull. Seismol. Soc. Am.* **97,** 76–90.

Wu, C., K. Koketsu, and H. Miyake (2008). Source processes of the 1978 and 2005 Miyagi-Oki, Japan, earthquakes: Repeated rupture of asperities over successive large earthquakes, *J. Geophys. Res.* **113,** no. B08316, doi: 10.1029/2007JB005189.

Wu, C., K. Koketsu, and H. Miyake (2009). Correction to "Source processes of the 1978 and 2005 Miyagi-Oki, Japan, earthquakes: Repeated rupture of asperities over successive large earthquakes," *J. Geophys. Res.* **114,** no. B04302, doi: 10.1029/2009JB006419.

Wyss, M. (1970). Stress estimates for South American shallow and deep earthquakes, *J. Geophys. Res.* **75,** 1529–1544.

Yagi, Y., and M. Kikuchi (2002). The source process of the Geiyo earthquake of March 24, 2001 obtained by joint inversion of teleseismic data and near-field data, *Seismol. Res. Lett.* **73,** 219.

Yokota, T., K. Ikeuchi, T. Yahagi, Y. Kaida, and H. Suzuki (2011). Attenuation and amplification of long-period component of ground motion, *J. Japan Assoc. Earthq. Eng.* **11,** no. 1, 81–101, doi: 10.5610/jaee.11.1_81 (in Japanese with English abstract).

Yokota, Y., K. Koketsu, Y. Fujii, K. Sataki, S. Sakai, M. Shinohara, and T. Kanazawa (2011). Joint inversion of strong motion, teleseismic, geodetic, and tsunami datasets for the rupture process of the Tohoku earthquake, *Geophys. Res. Lett.* **38,** L00G21, doi: 10.1029/2011GL050098.

Yuzawa, Y., and K. Kudo (2011). Empirical predictive model for long-period (1–15 s) ground motion on hard rocks, *J. Struct. Constr. Eng., AIJ* **76,** 519–526, doi: 10.3130/aijs.76.519 (in Japanese with an English abstract).

Earthquake Research Institute
University of Tokyo
1-1-1 Yayoi, Bunkyo-ku
Tokyo 113-0032
Japan

Manuscript received 14 August 2014;
Published Online 12 January 2016